NOVEL NON-INVASIVE TECHNOLOGY

FOR THE DETECTION OF THIN BIOFILM IN PIPING SYSTEMS

(PHASE – I)

by

Sachin Davis

A Thesis Submitted in

Partial Fulfilment of the

Requirements for the Degree of

Master of Science

in Engineering

at

The University of Wisconsin-Milwaukee

May 2019

ABSTRACT

NOVEL NON-INVASIVE TECHNOLOGY
FOR THE DETECTION OF BIOFILM IN PIPING SYSTEMS
(PHASE – I)

by

Sachin Davis

The University of Wisconsin-Milwaukee, 2019
Under the Supervision of Professor Marcia R. Silva

Biofilms are formed when a group of cells of microorganisms stick to each other and often on a surface. The development of biofilm has been a major issue in many fields (medical field, food, chemical, and water industry are a few such fields). In the medical field alone, biofilm infections have reportedly cost over five billion USD in additional healthcare expenses. The food industry usually halts the operation of its plant eight hours, every day to ensure that their equipment and transportation channels are clean and free from any biofilm presence. Similarly, the water and chemical industry needs to ensure that their transportation channels are free from biofilm build-up to ensure that the flow rate of liquid flowing through the channels are neither affected nor contain bacterial traces. There is an immediate need for new technologies, that are both real-time and non-invasive that can be used to quantify biofilm formation in closed systems, which can reduce the loss incurred by the healthcare, food, chemical and water industry.

This study investigates the use of a novel non-invasive and real-time technique that consists of two ultrasound sensors which can be mounted on a piping system. In this study, voltage and phase shifts were detected in materials with thickness greater than 40 μm, indicating that the sensor arrangement can be used to detect biofilm of thickness greater than 40 μm in a

closed piping system. The results of objects present in the closed system cannot be obtained using conventional techniques such as the Raman microscopy, confocal laser scanning microscopy (CLSM) or other microscopy methods. This technique also allows *in-situ* detection (i.e. it avoids the need for inserting or extracting a coupon from the medium for measurement and eliminates the need to obstruct the operation of the system or the flow of measurement media through the system).

To

my parents,

and professors.

TABLE OF CONTENTS

LIST OF FIGURES

LIST OF TABLES

ACKNOWLEDGMENTS

First and foremost, I would like to extend my sincere thanks to my advisor, Marcia R. Silva for recognizing my skills and potential to be involved in this research. She has helped cultivate in me a passion to give back to society. She has given me prompt guidance and help at the right time to keep the research moving in the right direction. Special thanks to Basil Hable and Ramprasad Karanam for their help and assistance provided for the success of this project and helping me in various stages of the research. I thank my thesis committee members Dr. Nathan Salowitz and Dr. Lucas Beversdorf for being an integral part of this research and their guidance on the scope of the research. I thank Alice Lecus and Matt Curtis for training me on the basics of using a Confocal Laser Scanning Microscope. I would like to extend my sincere gratitude towards the Water Equipment and Policy Center (WEP)/IUCRC for funding (Grant AAC9345) this research during its early stage. I also thank my industry mentors Luke Franklin (Dow), Mark Gehring (Dow), Steven Jons (Dow), Kun Xiong (Ecolab), Steve Hinterlong (Ecolab), Joe Bopp (Ecolab), Chen Li (AO Smith), Gusphyl Justin (AO Smith), and Kay Herbert (SLOAN), for their support and guidance throughout the project. Thanks to Randolf Metzger from UWM School of Freshwater (SFS) machine shop who was instrumental in helping me design and build the different testing chambers. Thanks to the UWM Innovation Campus team for helping me build a transparent testing platform that can be placed on the microscope.

I would like to thank my parents who encouraged me to pursue my dreams and turn me into the person that I am today. I have no idea where I would be today without their support and prayers.

Chapter 1

Introduction

1.1 Project Objectives

The objective of this research is to develop a device based on ultrasound technology that can non-destructively detect thin biofilm inside a piping system in real-time. The Phase I of this research and topic of this thesis is to conduct a proof of concept study to determine whether the sensors can detect the thin biofilm presence inside test chambers, constructed from different materials, that mimic a piping system.

1.2 Background

Biofilms were first described by Antonie van Leeuwenhoek. However, the process of the biofilm formation was not fully explained until 1978. J.W. Costerton et. al. [1] introduced the concept that bacteria stick, tenaciously and often with exquisite specificity, to surfaces ranging from the human tooth or lung and the intestine of a cow to a rock submerged in a fast-moving stream. They further noted that bacteria attach to surfaces by forming tangled fibres of polysaccharides often referred to as glycocalyx. The authors noted that this trend is observed in nature even though the bacteria covered by glycocalyx is not observed in laboratory cultures. The glycocalyx can also function as a food reservoir for bacteria. The polysaccharide fibres are for the most part negatively charged. Somewhat in the manner of an ion-exchange resin in the laboratory. they can bind nutrient ions and molecules that wander into the immediate environment or are produced by bacterial digestive enzymes, and thus keep them available to the cell [1]. Costerton and Lappin-Scott stated that the adhesion triggered expression of genes controlling production of

bacterial components necessary for adhesion and biofilm formation, emphasizing that the process of biofilm formation was regulated by specific genes transcribed during initial cell attachment [2]. Costerton et al., in 1987 [3], stated that biofilm consists of single cells and microcolonies, all embedded in a highly hydrated, predominantly anionic exopolymer matrix. Characklis and Marshall in 1990 [4] went on to describe other defining aspects of biofilms, such as the characteristics of spatial and temporal heterogeneity and involvement of inorganic or abiotic substances held together in the biofilm matrix. Biofilms, matrix–enclosed accumulation of dense microbial consortia living on biological or engineering surfaces, represent a significant and incompletely understood mode of growth for bacteria. Biofilms constitute a protected mode of growth that allows survival in a hostile environment. The structures that form in biofilms contain channels in which nutrients can circulate and cells in different regions of a biofilm exhibit different patterns of gene expression. The complexity of biofilm structure and metabolism has led to the analogy of biofilms to tissues of higher organisms [5]. Biofilm lifestyle adopted by nearly all bacteria in a myriad of environment can be dated back as early as nearly three billion years ago, which suggests that biofilm formation is an ancient and integral component of the prokaryotic life cycle and constitutes a key factor for survival of bacteria in diverse environments with many mechanical and chemical stressors. It is a known fact that bacteria can adhere to solid surfaces and form a slimy, slippery coat of extracellular polysaccharides which is otherwise referred to as extracellular polymeric substances (EPS). These bacterial biofilms are prevalent on most wet surfaces in nature and can cause environmental problems [6]. As ubiquitous as biofilms are, they impact many areas of human life, such as microbial infection related deaths, infections of medical devices, fouling of engineering surfaces, and even biodegradation of environmental pollutants.

Figure 1.1 shows a schematic diagram of the various stages of biofilm development for bacteria. Formation of biofilm is a sequential process, consisting of a series of steps that occur when cells encounter favourable nutrient and surface conditions.

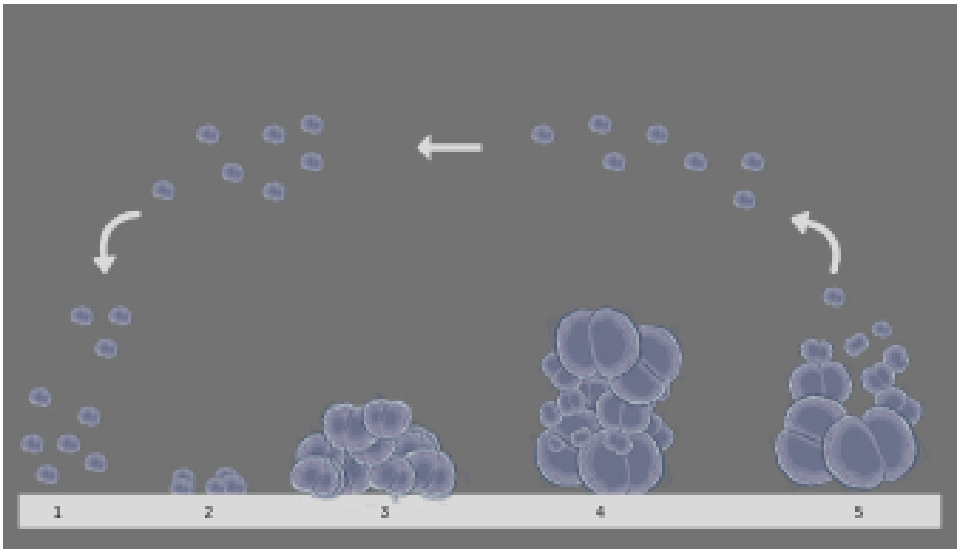

Figure 1.1: The five stages of growth (or colonization) of bacterial biofilms. The different stages of this growth are as follows: (1) Initial attachment, (2) Irreversible attachment, (3) Development of biofilm architecture, (4) Maturation of biofilm and (5) dispersion.

Biofilms are highly dependent on the environmental conditions and the surfaces colonized. The steps for the colonization of biofilms are briefly summarized as the following: (a) Stage 1: Initial attachment of cells to the surface. (b) Stage 2: Production of the extracellular polymeric substance resulting in more firmly adhered “irreversible” attachment. This stage as well as the next stage of biofilm colonization can be classified as ‘thin’ biofilms for this research. (c) Stage 3: Early development of biofilm architecture. (d) Stage 4: Maturation of biofilm architecture. (e) Stage 5: Dispersion of single cells from the biofilm [7]. Ricardo Murga et. al. performed quantitative analysis of biofilm thickness measurements and recorded the mean thickness of mono-population

biofilms of various bacterial strains [8]. This experiment points out that the mean initial thickness of mono-population biofilm is around 30 microns (or µm). The average thickness of *Pseudomonas aeruginosa* is 29 µm, *Klebsiella pneumoniae* is 100 µm and the average thickness of binary population biofilm is around 400 µm. At Stage 1, it is easy to clean the medium of any traces of bacterial cells. However, as the bacterial cells reach maturation i.e. Stage 4, the cleaning process becomes extremely difficult and strenuous. This means that advanced cleaning methods must be used to ensure that there are no traces of bacterial cells. This increases the cost of operation and can leave traces of chemicals or radiations which can later fuse with water or food particles and cause health hazards. The resistance of biofilms to industrial biocides were related to the property of limitation in mass transfer due to the matrix material [3]. It was then noted that the biofilm matrix limits diffusion only when the diffusing molecule reacts with the matrix material [9]. The biofilm phenotype was also found to be remarkably resistant to antibacterial agents, including antibiotics [10], and bactericidal effects of metal ions, including copper and silver. Different species of bacteria colonize the surfaces of these metals very avidly [11]. Intervention strategies currently used for biofilm control in the health industry (for medical devices) and the water industry will either:

- prevent initial device contamination,
- minimize initial microbial cell attachment to the device,
- penetrate the biofilm matrix and kill the biofilm-associated cells, or
- remove the device.

Extensive attempts to control biofilm formation in industrial systems by manipulation of the metallurgy and the surface characteristics of pipes and vessels have all failed. There is an equal lack of success if we take this approach with medical devices. Industry currently relies on mechanical cleaning and oxidative biocides. While the former removes biofilms, the latter gradually dissolves the biofilm matrix material and eventually kills the sessile cells [12]. However, the excessive use of the biocides (or other chemicals) may leave traces on the supply lines or piping systems. These traces can remain in the system and be dissolved in the liquid flowing through the piping system. The nature of biofilm structure and the physiological attributes of biofilm organisms confer an inherent resistance to antimicrobial agents, whether these antimicrobial agents are antibiotics, disinfectants, or germicides. Table 1 shows the differences in susceptibility of planktonic and biofilm organisms to antimicrobial agents [12].

Mechanisms responsible for resistance may be one or more of the following:

- delayed penetration of the antimicrobial agent through the biofilm matrix,
- altered growth rate of biofilm organisms, and
- other physiological changes due to the biofilm mode of growth.

Table 1: Susceptibility of planktonic and biofilm bacteria to selected antibiotics. The concentrations of planktonic phenotype are minimum inhibitory concentration (MIC) or minimum bactericidal concentration). The strains described in the table below are National Collection of Type Cultures (NCTC) and American Type Culture Collection (ATCC).

Organism	Antibiotic	Concentration of Planktonic Phenotype (µg/ml)	Concentration effective against biofilm phenotype (µg/ml)
Staphylococcus aureus NCTC 8325-4	Vancomycin	2.000 (MBC)	20.00 (for 99% reduction) [13]
Pseudomonas aeruginosa ATCC 27853	Imipenem	1.000 (MIC)	>1,024.00 (for minimal eradication concentration) [14]
Escherichia coli ATCC 25922	Ampicillin	2.000 (MIC)	512.00 (for 99% reduction) [14]
Pseudomonas pseudomallei	Ceftazidime	8.000 (MBC)	800.00 (for 99% reduction) [15]
Streptococcus sanguis 804	Doxycycline	0.063 (MIC)	3.15 (for 99.9% reduction) [16]

Biofilms are a huge problem in many industries. Healthcare, water, and food are a few such industries where this issue is widely seen. In the food industry, biofilm formation has been a major problem leading to a loss of profits and high downtime. The Center for Disease Control and Prevention (CDC) estimates that approximately 48 million people get sick, 128,000 are hospitalized and 3,000 die each year due to food-related illnesses throughout the United States, which are often referred to as food poisoning. According to the model developed by researchers at the John Hopkins Bloomberg School of Public Health, a fast food restaurant could incur anywhere from 4,000 USD for a single outbreak in which five people get sick (when there is no loss in revenue and no lawsuits, legal fees, or fines are incurred) to 1.9 million USD for a single outbreak

in which 250 people get sick (when restaurants loose revenue and incur lawsuits, legal fees, and fines) [17]. Biofilms form not only on processing environment surfaces but also on the food itself, offering potential for cross-contamination and post-process contamination. Developments such as the demand for minimally processed foods have placed a renewed emphasis on good hygienic practices in the food industry. It is said that the food industry stops its process every day for about eight hours for cleaning the conveyors and the vessels. If the amount of biofilm formation is known, then the time for cleaning can be adjusted accordingly, thus saving both money and time. Hospitalizations for three common waterborne diseases cost the health care system as much as 539 million USD annually, according to research presented at the International Conference on Emerging Infectious Diseases [18]. Inpatient hospitalization costs per case averaged more than 34,000 USD for Legionnaires' disease, approximately 9,000 USD for giardiasis and more than 21,000 USD for cryptosporidiosis. When people think about these diseases, they usually think of a simple case of diarrhoea, which is a nuisance but quickly goes away. However, these infections can cause severe illness that often result in hospital stays of more than a week, which can quickly drive up health care costs. Some common symptoms of waterborne diseases can include rashes, eye and ear infections, respiratory or neurological symptoms and sometimes can be fatal [18].

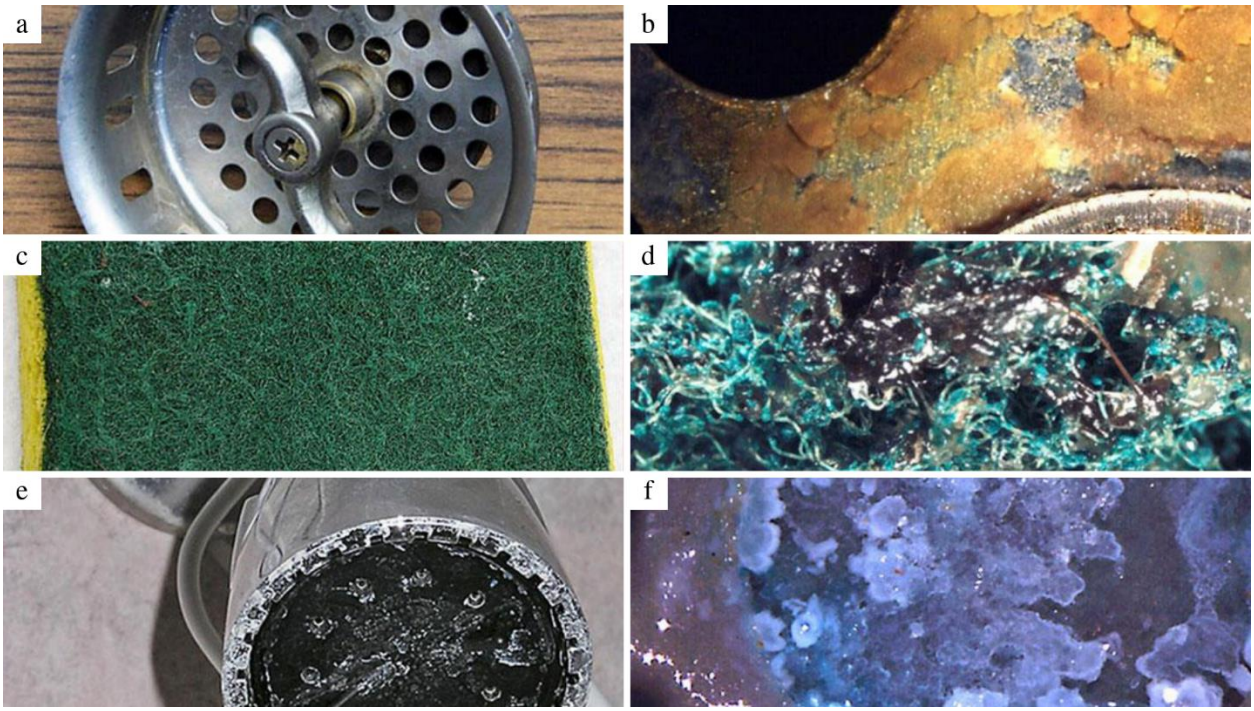

Figure 1.2: Biofilms encountered in everyday objects when observed under the stereo microscope. (a) kitchen strainer, (b) strainer as observed with a stereo microscope, (c) kitchen sponge, (d) kitchen sponge as observed with a stereo microscope, (e) shower head and (f) shower head observed with the microscope. (Source: Montana State University - Center for Biofilm Engineering (MSU CBE), 2006)

A range of more advanced approaches has been employed to quantify various aspects of biofilm formation over a transparent wall, yet no technique currently exists that can image biofilm formed over opaque boundaries such as biofilm build-up within city water network. It is highly desirable to have reliable, fast and high spatial resolution visualization techniques capable of resolving sub-matrix. In literature, several 3D microscopic methods have been developed: e.g. Confocal Laser Scanning Microscopy (CLSM), digital holographic microscope (DHM) [19] and Berg's Tracking Microscope [20]. Figure 1.2 shows an image of everyday objects and the biofilm presence in these objects when observed under a stereo microscope. J. Sheng et. al. [19] introduced the application of DHM to measure sub micro-meter (0.75 μm) particles in dense liquid suspensions with depths of 1 – 10 mm. The sample is illuminated with a collimated laser beam

and the magnified image of the optical field created on a plane outside of the sample volume is recorded digitally. The recorded image is a magnified digital in-line hologram. Molaei et al. [21] developed a microfluidics + DHM platform for measuring the 3D motion of bacteria while resolving the cell shape and orientation. The authors applied DHM to track swimming bacteria in three dimensions. Bacteria are considerably more difficult to image with DHM compared to other objects previously imaged with this method, including larger plankton cells. These cells have a smaller refractive index (n = 1.35) compared to that of water (n = 1.33). Careful optimization of the imaging optics helped succeed in the successful usage of imaging approximately 3000 wild-type *Escherichia coli* (*E. coli)* bacteria over the entire 200 µm depth of a microfluidic device, with a spatial resolution of 0.2 µm (lateral) and 0.5 µm (axial). By enabling simultaneous tracking of large number of cells without any moving parts in the setup, this approach establishes DHM as a powerful technique for tracking bacteria. However, it fails to visualize thick biofilm or film formed over the opaque surface. The 3D tracking microscope uses a standard phase contrast microscope and a camera for data acquisition. Dozens of trajectories are acquired simultaneously using this method and enhanced tracking range in z- axis enables acquisition of significantly longer 3D trajectories for unconfined cells. This technique captures bacterial motility in a broad range of contexts from microfluidic platforms to complex 3D environments like those encountered in nature [22]. L. Turner et. al. developed a procedure where individual cells were imaged in phase contrast and characterized the track of cells by measuring run and tumble speeds (µm/s), run and tumble intervals (s), angular speeds while running and tumbling (°/point), the change in direction from run to run (°), and the change in direction during runs (°) [23]. The method developed by them can be seen in Figure 1.3.

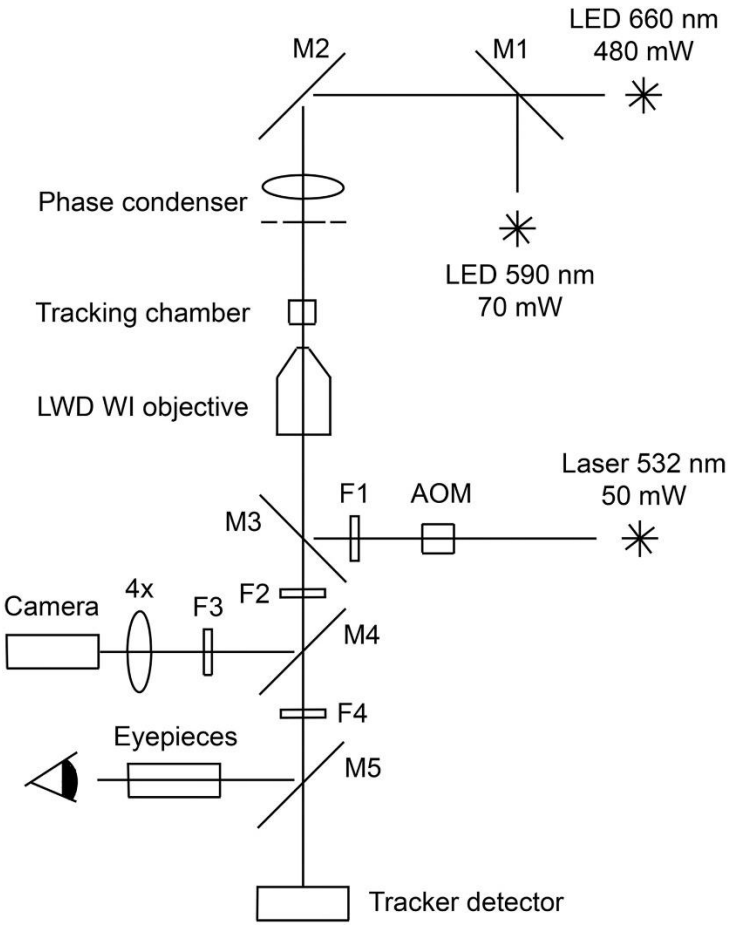

Figure 1.3: Tracking microscope optical paths. Laser lights are used to track the cells in this method [21].

Another common method used for the detection of biofilm is the CLSM. CLSM is a valuable tool for the study of biofilms, and of the biofilm matrix, as it allows real-time visualization of fully hydrated, living specimens. Over the years, methods based on CLSM have evolved considerably in the past decade to retrieve information about the composition and the properties of the biofilm matrix [24]. The CLSM method is more effective when a biofilm (or bacterial cell) is stained with a standard dye. Nile red stained cell techniques were used to observe bacterial cells with the confocal laser scanning microscope. R. Zuriani et. al studied the throughput means to measure the fluorescence intensity of Nile red stained cells containing polyhydroxyalkanoate

(PHA). The concentration of PHA was determined using the Nile red dye by establishing a linear correlation between the fluorescence intensity and intracellular PHA concentration [25]. N. Kamjunke et. al. [26] has developed a modified approach to enable CLSM analyses of undisturbed biofilms on paints under field conditions by using painted polycarbonate slides. Quantitative analysis of top-view CLSM data is possible for thin biofilms only since emitted light do not pervade thick biofilms. Biofilm thickness measured from cryosections was positively related to biomass dry weight but not to the vertical extension of CLSM top-view images indicating that the preparation of cryosections is necessary to investigate thick biofilms. The confocal microscopy is usually used for Geometric measurements, Solute concentration measurements and Diffusion properties measurement. The geometric measurements are conducted by measuring the area/volume quantification of fluorescently stained matrix components using digital image analysis [27] [28] and colocalization analyses of bacteria and matrix components using digital image analysis [29]. The measurements of solute concentrations are achieved by the immobilization of pH/O_2- sensitive fluorescent dyes in particles [30] [31], Fluorescence lifetime imaging (FLIM) of pH- sensitive fluorescent dyes [32] and pH ratiometry [33] techniques. The measurements of diffusion properties are achieved by Time-lapse imaging [34], Single particle tracking [35] [36], Fluorescence recovery after photobleaching [37] [38] and Fluorescence correlation spectroscopy [38] [39]. However, the limitation of using these techniques is that these methods are both destructive and has a slower turn-over time. This implies that a coupon is inserted into the system to gather the bacterial matrix (or biofilm particles) and taken to the laboratory for testing. The results from the oscilloscope can be obtained only after 12 or more hours. Table 2 shows a brief summarization of the strengths and limitations of the above technology and the

advantage of using Ultrasound technology over these methods. Other non-invasive detection strategies include the Microtiter plate. Biofilm formation in microtiter plates is certainly the most commonly used method. Originally developed by Madilyn Fletcher to investigate bacteria attachment [40], the bacterial cells are grown in wells of a polystyrene microtiter plate. At different time points, the wells are emptied and washed to remove planktonic cells before staining the biomass attached to the surface of the wells, to measure all attached biomass. However, parts of biomass may stem from cells sedimented to the bottom of the wells, and subsequently embedded by EPS [41]. To overcome the biomass accumulation, the Calgary biofilm device was developed where the biofilm formation is assayed at the coverlid, composed of pegs that fit into the wells of the microtiter plate containing the growth medium and bacteria. The biofilm formed on the pegs does not result from cell sedimentation but only from sessile development [42]. A method for investigating early stages of biofilm development is the Biofilm Ring Test [43] based on the capacity of bacteria to immobilize microbeads when forming a biofilm at the surface. The bacterial suspension is mixed with paramagnetic microbeads before being loaded into the wells of a microtiter plate. The plate is then incubated, and direct measurements can be performed at different time points, without any staining and washing steps. The more biofilm, the less the beads can move when a magnetic field is applied [43]. Alternatively, the Robbins device based on the design of Jim Robbins and Bill McCoy, later patented in a revised version by the Shell Oil Company [44] can be used to estimate the quantity of biofilm. It consists of a pipe with several threaded holes where coupons are aligned parallel to the fluid flow and can be removed independently. The original Robbins device was used to monitor biofilm formation under different fluid velocities in a simulated drinking water facility [45].

Table 2: The strengths and limitations of some invasive technology like CLSM, Raman microscopy, Surface Enhanced Raman spectroscopy, Fluorescence in situ Hybridization (FISH) and other non-invasive technology like optical coherence tomography and ultrasound. EPS stands for Extracellular polysaccharides.

	Strengths	Limitations
Invasive Technology		
CLSM [46]	State of the art technique for characterizing biofilm	Requires staining of all parts of EPS which is practically impossible, Time consuming, Incompatible design, Increased costs for supporting equipment.
Raman Microscopy [46]	No staining of EPS required	Slower than CLSM Method, Incompatible design, Increased cost for other supporting equipment.
Surface Enhanced Raman Spectroscopy [47]	Can be used for the detection of biofilm material present in lower concentrations	Use and preparation of chemicals is both tedious and time-consuming, Incompatible design, Increased cost for additional equipment, Slower than Raman microscopy method.
Fluorescence in situ Hybridization (FISH) [48]	Used for detailed study on the biofilms	Limitation to observe environmental samples as they relate to rocks, clays and sediments, use of this technique is hindered by strong autofluorescence of phototrophic microorganisms.
Non-invasive Technology		
Optical Coherence Tomography [49]	Very fast results	Used for analysis of biofilm in mid-ear, uses near infrared light source, not easily compatible, requires the device to be inserted into the medium for biofilm observation.
Ultrasound Imaging [50]	Proven method for more than 50 years (especially medical field)	Fast results, non-destructive testing strategy, detection of biofilm requires no need for costly equipment.

The physiology of single cells and the interactions inside a biofilm have been analysed at increasingly higher level of detail facilitated by the development of new and better hardware tools, such as microfluidics and high-resolution microscopy. The molecular tools are also becoming far more refined and accessible than before, allowing physiological dissection of small, distinct entities within the complex biofilm structures [51]. However, all these methods are time-consuming since it involves the preparation of bacterial cells.

Materials like plastics or polymers can be used to simulate biofilm thicknesses since using these materials takes less preparation time when compared to prepare bacterial cells. However, plastics are not a good biofilm models since most plastics are not as porous as biofilm. Polymers on the other hand can be created to have similar properties to biofilm. They can be prepared with ease and the thickness of these materials can be adjusted using a spin coater. One such polymer is the Poly (dimethyl siloxane) (PDMS), which is a nontoxic silicone with unique flow properties that lend it to widespread applications, from biomedical devices to food, automobiles, and even home construction [52]. PDMS belong to a group of polymeric organosilicon compounds which are commonly referred to as "silicones". These are clear, colourless and odourless liquids that have non-detectable vapor pressure and are insoluble in water. They are also non-toxic and non-flammable [53]. Another material that is used for the simulating the presence of biofilm is agarose beads [91] or porous beads or simply agar-based gels. M. Strathmann et. al. [91] developed a super porous agarose bead by a double emulsification procedure. 100 ml of an agarose solution was prepared by heating a suspension of agarose in water to 95 – 100 ºC in a water bath. In some samples, bacterial suspensions were added to create a live super porous bead that was visualized using the confocal laser scanning microscope. However, in this research, Poly-2-hydroxyethyl

methacrylate (PolyHEMA) was used as a substitute for biofilm to simulate results because PolyHEMA is easier to prepare when compared to PDMS and is more porous thus resembling biofilm more. PolyHEMA is a soft, flexible, water-absorbing plastic used to make soft contact lenses. It is a polymer of 2-hydroxyehtyl methacrylate (HEMA), a clear liquid compound obtained by reacting methacrylic acid with ethylene oxide or propylene oxide. HEMA can be shaped into a contact lens by being cast into a small, conclave, spinning mould. Under the influence of heat or light and free-radical initiators, the HEMA polymerizes, and its molecules link together to form long, multiple-unit chains [54]. The elemental mapping analysis of the hybrid nanocomposite poly (hydroxyethyl methacrylate-*co*-methyl methacrylate)-*g*-polyhedral oligosilsesquioxane [poly (HEMA-*co*-MMA)-*g*-POSS.], using X-ray photoelectron spectroscopy and Energy-dispersive X-ray suggest the formation of poly (HEMA-co-MMA) -anchored POSS nanocomposites [55]. Minett T. W et. al. [56] investigated the topography of PolyHEMA coated culture substrates by scanning electron microscopy, and quantitatively assessed their effect upon the spreading activity of mammalian cells. Results indicated a clear correlation between cell spreading activity and polymer film discontinuity. Preparation of PolyHEMA films on modified tissue culture substrates allowed direct investigation of the role of the underlying substrate in regulating cell spreading and confirms that apparent modulation of cell spreading by PolyHEMA reflects increasing expression of the coated surface. The authors further employed a spinning technique by which films of precise thickness, down to 0.01 micron, may be produced on coverslips. All PolyHEMA coatings prepared in this way are smooth, complete and do not allow cell attachment at any thickness. The authors concluded that PolyHEMA is non-adhesive for mammalian cells [56].

In 1974, Lazzaro Spallanzani proved that bats can navigate accurately in the dark through echo reflection from high frequency inaudible sound. Richardson invented the echo locator in 1912 based on the idea of ultrasound used for navigation and detection of objects in the water. Later, Paul Langevin created the first technological application of ultrasound to detect submarines and a pulse-echo ultrasonic metal flaw detector was constructed in 1930 [47]. Ultrasound was first used for clinical purposes in 1956 in Glasgow. Obstetrician Ian Donald and engineer Tom Brown developed the first prototype systems based on an instrument used to detect industrial flaws in ships. One of the main advantages of ultrasound is that it is non-invasive. At current levels, ultrasound is safe for clinical investigations but at high power, ultrasound waves can damage tissue issue [48]. The beginning of Sonar and ultrasound for medical imaging is traced back to the sinking of the Titanic. Within a month of the Titanic tragedy, British scientist L.F Richardson (1913) filed patents to detect icebergs using ultrasound. French scientists Chilowski and Langevin started developing device to detect submarines using Ultrasound during World War 1 [57]. Ultrasound has been widely used in industrial applications to detect defects in structures and to provide biomedical imaging of cells, tissues, and organs. Ultrasound is now a useful and flexible modality in medical imaging and often provides an additional or unique characterization of tissues. An ultrasound transducer sends an ultrasound pulse into tissue and then receives echoes back. The echoes contain spatial and contrast information. The concept is analogous to sonar used in nautical applications, but the technique in medical ultrasound is more sophisticated, gathering enough data to form a rapidly moving two-dimensional grayscale image. Some characteristics of returning echoes from tissue can be selected out to provide additional information beyond a grayscale image. Doppler ultrasound, for instance, can detect a frequency shift in echoes, and determine whether

the tissue is moving toward or away from the transducer. This is invaluable for evaluation of some structures such as blood vessels or the heart (echocardiography) [58]. A. Aubry et. al. developed experimental set up which uses an array of sources/receivers placed in front of the medium. The impulse responses between every couple of transducers were measured and formed into a matrix. Single-scattering contributions are shown to exhibit a deterministic coherence along the antidiagonals of the array response matrix, whatever the distribution of inhomogeneities. This property is taken advantage of to discriminate single from multiple-scattered waves. Experimental results were observed with ultrasonic waves in the MHz range, on a synthetic sample (agar-gelatin gel) as well as on breast tissues. The authors found that the multiple scattering contribution is negligible in the breast around 4.3 MHz [59]. The attenuation of sound waves and the dispersion of waves in cancellous bones in humans were studied with the help of ultrasound. The experiments were performed with a bone model that mimics phantom and human cancellous bones. The focus of the experiment was based on the analysis of physical mechanisms of ultrasonic wave propagation in cancellous bone that govern phase velocity and attenuation coefficient as function of frequency and porosity [60]. The properties of a liquid such as the viscosity and absorption are especially important for acoustic investigations because these factors affect the proper choice of the measuring method and temperature−pressure conditions. Ionic liquids (ILs) are generally much more viscous than conventional molecular organic liquids, i.e., the viscosity values of most ILs at room temperatures are two to three orders of magnitude larger than almost all molecular organic liquids. The propagation terms in most ILs are rather like those in highly associated viscous polyhydroxyl liquids compared to those in low-viscous conventional molecular organic liquids [61]. Ultrasonic Testing (UT) uses high frequency sound energy to conduct examinations and

make measurements. Ultrasonic inspection can be used for flaw detection/evaluation, dimensional measurements, material characterization, and more. A typical UT inspection system consists of several functional units, such as the pulser/receiver, transducer, and display devices. A pulser/receiver is an electronic device that can produce high voltage electrical pulses. Driven by the pulser, the transducer generates high frequency ultrasonic energy. The reflected wave signal is transformed into an electrical signal by the transducer and is displayed on a screen as shown in Figure 1.4. The reflected signal strength is displayed versus the time from signal generation to when an echo was received, and the signal can sometimes be used to gain information about the features of a defect [62].

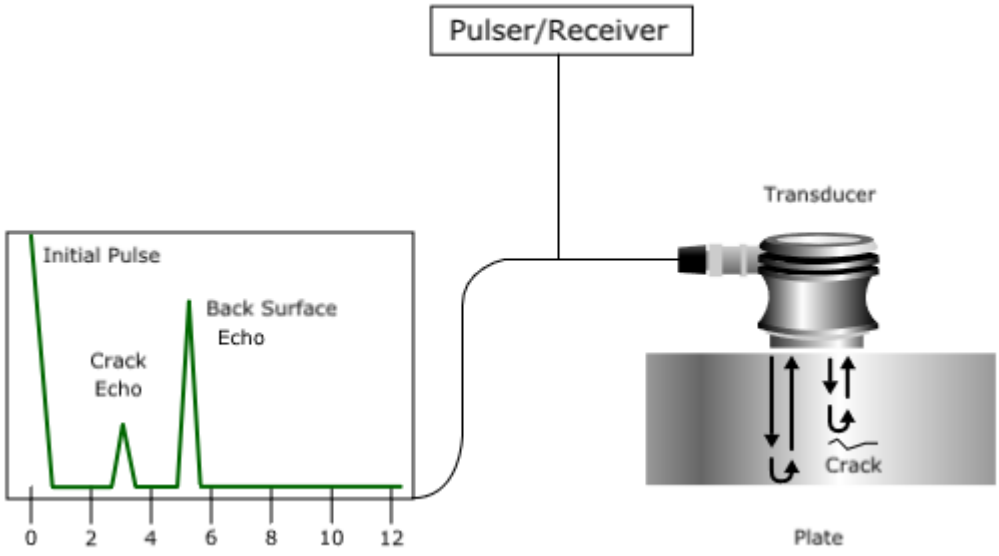

Figure 1.4: Ultrasonic detection technique illustrated by a single ultrasound sensor and a solid surface with an internal crack and an oscilloscope screen portraying signals showing information about the approximate position and size of the defect (Source: NDT Resource Center, www.nde-ed.org).

Ultrasound waves can propagate in four principle modes that are based on the way the particles oscillate. Sound can propagate as longitudinal waves, shear waves, surface waves, and in thin materials as plate waves. Longitudinal and shear waves are the two modes of propagation most widely used in ultrasonic testing. The particle movement responsible for the propagation of longitudinal and shear waves is shown in Figure 1.5.

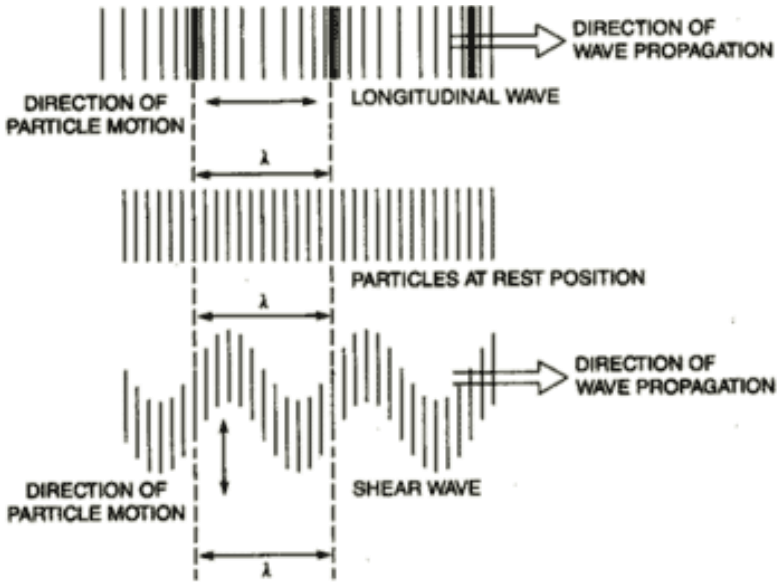

Figure 1.5: Particle movement for the propagation of longitudinal and shear waves. The longitudinal waves occur in the direction of wave propagation and the shear waves have oscillation at right angles to the direction of propagation (Source: NDT Resource Center, www.nde-ed.org).

In longitudinal waves, the oscillations occur in the longitudinal direction or the direction of wave propagation. Since compressional and dilatational forces are active in these waves, they are also called pressure or compressional waves. Compression waves can be generated in liquids, as well as solids because the energy travels through the atomic structure by a series of compressions and expansion (rarefaction) movements. In the transverse or shear wave, the particles oscillate at a right angle or transverse to the direction of propagation. Shear waves require

an acoustically solid material for effective propagation, and therefore, are not effectively propagated in materials such as liquids or gasses. Shear waves are relatively weak when compared to longitudinal waves [63]. The principle of ultrasound is based on the reflection and refraction properties of sound. Reflection of a sound wave occurs when the wave passes between materials of different acoustic speeds and a fraction of the wave bounces back. Like light, the incoming incident wave bounces off the boundary at an angle of incidence (θ_i) which is equal to the angle of reflection (θ_r) or $\theta_i = \theta_r$ as seen in Figure 1.6.

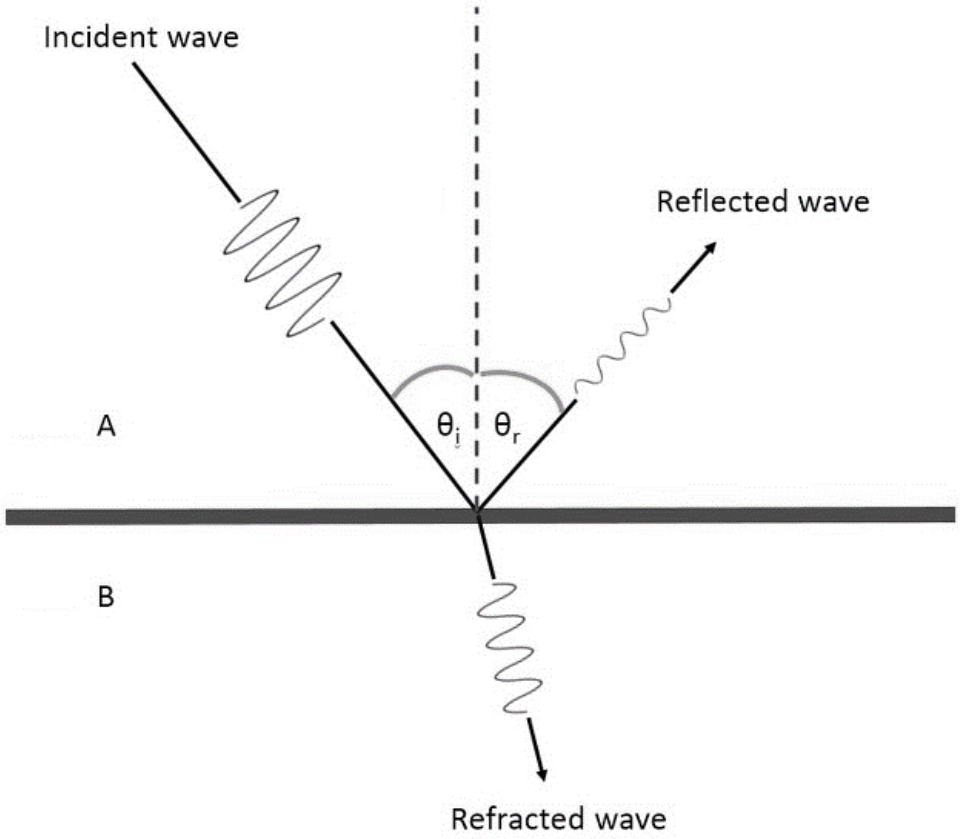

Figure 1.6: Reflection property of sound. It can be observed that the angle of the incident wave is equal to the angle of the reflected wave (Source: Courtesy of Dr. Yuranga Weerakkody and Dr. Jeffrey Chang, Radiopaedia [64]).

This contrasts with reflection where the angles of incidence and refraction may not be equal dependent on the acoustic impedance of material and the refractive indices of the medium through which sound travels. The intensity of the reflected wave is defined by the reflection coefficient (R_I) which is equal to the intensity of the incident sound wave (I_i) divided by the intensity of the reflected sound wave (I_r) i.e. $R_I = {}^{I_i}/_{I_r}$. The transmitted intensity (T_I) is the energy that is transmitted through the boundary and this represents all the energy from the incident sound wave which was not reflected i.e. $T_I = 1 - R_I$. However, the air interaction between the transducer and the medium makes almost 99% of the sound wave reflect off the interface. This is the reason an ultrasound gel must be used on transducers to remove any pockets of air [64]. Refraction of sound wave occurs when it travels between mediums with different propagation speeds or refractive indices. As the incident wave strikes a surface of different refractive index, the direction of the wave changes [65] according to Snell's law as described for light by the Dutch astronomer and mathematician Willebrord Snell in 1621. If θ_1 is the incident angle of the sound wave at the interface with refractive index n_1 and θ_2 is the refraction angle of the sound wave in the new medium with refractive index n_2, then $\frac{n_1}{n_2} = \frac{\sin(\theta_2)}{\sin(\theta_1)}$. The change in direction can be seen in Figure 1.7. When the sound waves travel from a denser medium to a medium with higher refractive index, the refracted wave bends towards the normal line (indicated by dotted lines in Figure 1.7) and when sound travels from a rarer medium to a denser medium, the refracted wave bends away from the normal line.

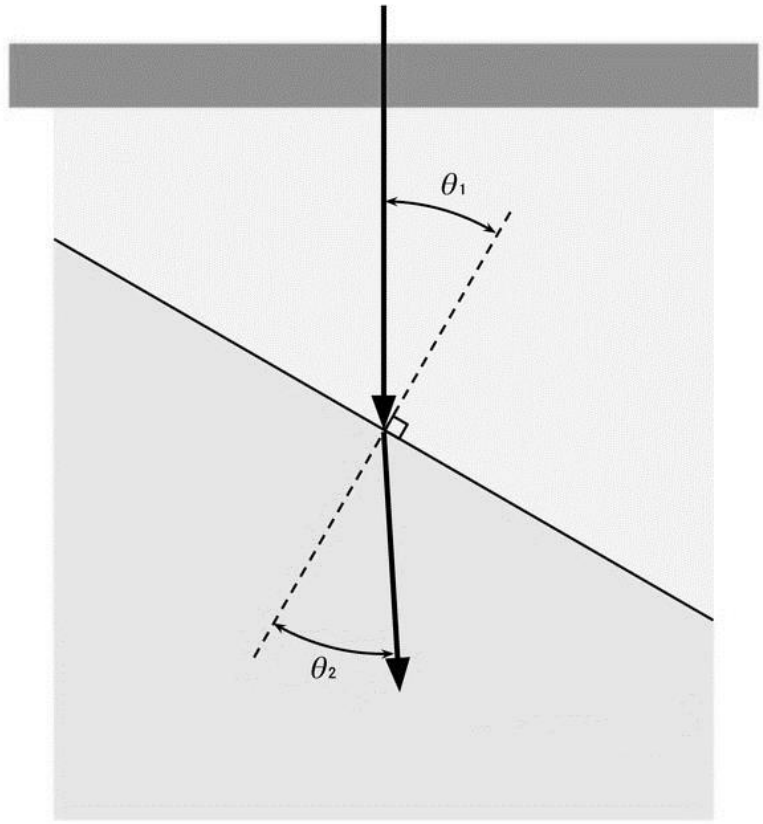

Figure 1.7: Refraction of sound waves at two interfaces. The light gray region represents a medium with lower refractive index when compared to the medium represented by the darker gray region (Source: Courtesy of Dr. Henry Knipe and Dr. Patricia O'Gorman, Radiopaedia [65]).

Ultrasound techniques have been used for the detection of cracks in solid surfaces for quite a few years. An ultrasound sensor is placed on the solid surface and ultrasound signals are passed through the surface and the reflected signals are recorded with the help of an oscilloscope. When there is no crack or defect inside the solid surface, the wave reflects to the sensor after a fixed interval. However, if there is a crack or a defect, a second wave can be detected at an earlier interval with a smaller amplitude (shown in Figure 1.4). Originally, rail inspections were performed solely by visual means. Visual inspections will only detect external defects and sometimes the subtle signs of large internal problems. The National Transportation Safety Board established that the rail

failure was caused by a defect that was entirely internal and probably could not have been detected by visual means. Nowadays, ultrasonic testing technique has been used in railroad inspections since they provide means to detect internal defects [66]. Being capable of imaging through opaque or solid materials, the ultrasound techniques often lower spatial resolutions and provide faster results. Several methods have been developed that is able to measure the amount of biofouling (or biofilm) in piping systems or on surfaces. S.T.V Sim et. al [67] developed a method to detect biofouling in reverse osmosis systems. Jianxin Li et. al. [68] used a similar method as shown in Figure 1.4 to detect membrane fouling. However, these methods only use a single ultrasound sensor and relies on the back echo of the sound wave to detect the presence of biofilm. This technique is like that shown in Figure 1.4. While these methods confirm the ability of ultrasound sensors to detect the presence of biofouling, these methods are less accurate compared to the method incorporated in our research.

In this research, 'thin' biofilms are considered as those that are in Stage 3 or less (that is, 30 microns or less). The aim of this study is to detect the biofilm at their early stage of development when their response to cleaning agents has not been developed. Two ultrasound sensors are placed on either side of the plastic chamber and the presence of a test object (made from materials inside the laboratory), presence of biofilm or presence of PolyHEMA is interpreted using the signal received from receiver ultrasound sensor. The advantage of using two ultrasound sensors for the detection of fouling is that it is more accurate than the single ultrasound measurement method since the sound wave experiences less attenuation since the distance that the sound wave travels is comparatively low. The transmitter sensor is powered by a function generator that can output constant eight burst signals of 1 MHz frequency. The effect of dissolved solids and the effect of

different materials are also tested to understand the change in sensor data due to these phenomena. In this research, the effect of sensor data is also tested as the number of dissolved solids in the test chamber increases and the changes in the sensor output as the materials of the test chamber is changed. The correlation analysis on different trials for the experiment related to biofilm and solubility test indicated that there is a change in voltage and phase shift as the thickness of the contaminant on the inner wall of the system being measured increases. The PolyHEMA experiment displayed a similar trend where the voltage and phase output decreased as the thickness of the solidified PolyHEMA increased. However, the agar experiment (where pure agar with no doping of substances) displayed a trend of increasing voltage since the agar-based gel acted as a perfect medium for sound to travel from the transmitter to the receiver.

1.3 Significance and Novelty

The significance of this research is the development of a non-invasive technology capable of detecting thin biofilms in the inner walls of water supply pipes. The advantages of this technique over existing technique is that the size and cost of the system can be greatly reduced, while producing valid and reliable results. The sensors also produce data in real-time thus eliminating the need to wait for a long time to identify the presence of bacterial biofilms in piping systems. The device developed incorporating the use of the two-ultrasound sensor can be easily mounted onto a piping system and readings can be taken instantaneously.

The novelty of the detection method being developed is that it requires no need for secondary methods to validate the receiver data and requires sensors with lower frequency compared to 20 MHz ultrasound sensor [69]. This technique also requires two ultrasound sensors which provides better results in comparison with a single sensor which uses reflection method for

the detection of biofilm [70] [71]. When the ultrasound wave is reflected from a surface, the wave undergoes higher attenuation (since it travels twice the distance) in comparison with the method used in this research where the ultrasound waves are captured before undergoing further attenuation. Bierganns, Patric et. al. has developed two patented methods [72] [73] which use ultrasound theory for the detection of deposits. However, these methods require secondary detection methods to confirm the data obtained by the ultrasound sensor. The secondary methods for the two patents are chemical imaging sensors (or a light addressable potentiometric sensor) or a temperature sensor. In the method involving a temperature sensor, a heater arrangement is included along the surface of the material where the deposits are to be detected. The patents reinforce the idea that the presence of deposits can be analyzed (or determined) by using an ultrasound transmitter and receiver. However, the secondary methods discussed above requires additional hardware thus increasing the spatial requirements and cost of the overall device. The technology (both economical and cost effective) being developed through this research can be used for the detection of biofilm inside water pipes to ensure that clean water is accessible to all human beings.

Chapter 2

Materials

2.1 Sensors and Evaluation boards

2.1.1 Sensors used in the research

The sensors used in various stages of this research are a series of ultrasound sensors with various frequencies. The sensors and their specifications are as follows:

(a) 1 MHz Ultrasound sensor (1ME21TR-1, Osenon Technology)

The 1ME21TR-1 has the functions of transmitter and receiver. It generally can be used for ultrasonic flow sensor, ultrasonic calorimeter, ultrasonic sensor for non-contact detect objects, ultrasonic distance sensor in liquid, etc. [74]. These sensors are dual-use sensors and can be used as both a receiver and/or transmitter. The characteristics of the sensor is shown in Table 1.

Table 3: The characteristics of the 1 MHz ultrasound sensor (1ME21TR-1)

Nominal Frequency	1.0 MHz ± 5%
Bandwidth	200.0 kHz
Max. Input Voltage	300 V_{pp}
Directivity and Sensitivity	8° ± 2° (-6dB), -35dB (min.)
Protection Level and Material	IP65, Plastic
Maximum Pressure	1.6 MPa
Operating Temperature	-20 °C ~ +80 °C
Distance of Detection	0.1 ~ 5 m (reflection in liquid)

Figure 2.1 shows the 1 MHz ultrasound sensor. This ultrasound sensor is manufactured and sold by Osenon Technology. The sensor is activated by connecting to a function generator that can output an eight-burst signal with a voltage of 3 V_{pp}. Some of the features of this sensor are as follows [18]:

- Small size and light-weight
- High sensitivity and high sound pressure
- Low power consumption and
- High reliability

Figure 2.1: 1 MHz (1ME21TR-1) Ultrasound sensor (Source: osenon.com).

(b) 40 kHz Ultrasound sensor (HC-SR04)

The HC-SR04 ultrasonic sensor (shown in Figure 2.2) uses sonar to determine distance to an object like bats or dolphins do. It offers excellent non-contact range detection with high accuracy and stable readings in an easy-to-use package. From 2 to 400 cm or 1" to 13 feet. The operation of this sensor is not affected by sunlight or black material like Sharp rangefinders are

(although acoustically soft materials like cloth can be difficult to detect). It comes complete with ultrasonic transmitter and receiver module [75]. The features of the ultrasound sensor can be seen in Table 2.

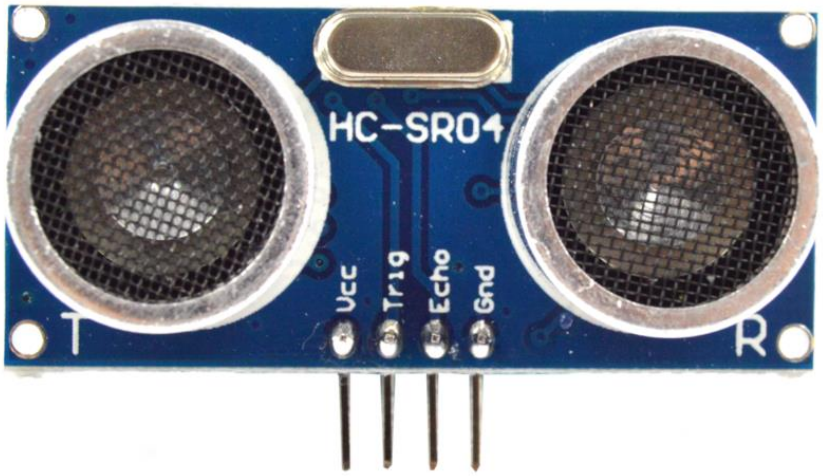

Figure 2.2: 40 kHz (HC-SR04) Ultrasound sensor (Source: robotshop.com).

The four pins of the ultrasonic sensor are V_{cc}, Trig, Echo and GND. The V_{cc} pin of the ultrasound module must be connected to 5 V DC signal, the Trig pin is the Trigger input of the sensor, the Echo pin provides the Echo output of the sensor and the GND pin must be connected to ground. To start measurement, Trig pin of HC-SR04 must receive a pulse of high (5 V) for at least 10us, this will initiate the sensor will transmit out eight cycle of ultrasonic burst at 40 kHz and wait for the reflected ultrasonic burst. When the sensor detected ultrasonic from receiver, it will set the Echo pin to high (5 V) and delay for a period (width) which proportion to distance. To obtain the distance, measure the width of Echo pin [75].

- Time = Width of Echo pulse, in µs.
- Distance in centimetres = Time / 58

Table 4: Features of the Arduino compatible HC-SR04 ultrasonic sensor

Power Supply	5 V DC
Working Current	15 mA
Effectual Angle	< 15°
Ranging Distance	2 – 400 cm
Resolution	0.3 cm
Measuring Angle	30°
Trigger Input Pulse Width	10 µs

2.1.2 Evaluation boards used in research

The sensor output was evaluated using two different methods: one method involving the oscilloscope and the other involving evaluation boards. The evaluation boards can activate the transmitter sensor and enable the user to observe the data from the receiver sensor. The evaluation boards used in this research and their specifications are as follows:

(a) Texas Instruments Time to Digital Converter (TDC) 1000-7200 EVM Board

The TDC1000-TDC7200EVM (as shown in Figure 2.3) is an evaluation module (EVM) that allows users to evaluate the operation and performance of the TDC1000 ultrasonic analogue-front-end with TDC7200 time-to-digital converter. The board can be used for many time-of-flight applications such as gas, water, and heat flow meter, fluid level detection, concentration and fluid identification, and proximity or distance measurements. The EVM allows for two ultrasonic transducer connections, and two RTD connections for temperature measurements. It uses the on-board MSP430F5528 to process data and a user-friendly GUI interface to display the data [76].

Figure 2.3: TDC1000 - TDC7200 EVM Evaluation board (Source: ti.com).

The features of the EVM are as follows:

- User friendly GUI interface
- On-board MSP430F5528 to process data
- Connectors for two ultrasonic transducers, and connectors for two RTD sensors
- Powered by USB

The TDC1000 is a fully integrated analogue front-end (AFE) for ultrasonic sensing measurements of level, fluid identification/concentration, flow, and proximity/ distance applications common in automotive, industrial, medical, and consumer markets. TI's Ultrasonic AFE offers programmability and flexibility to accommodate a wide-range of applications and end equipment. The TDC1000 can be configured for multiple transmit pulses and frequencies, gain, and signal thresholds for use with a wide-range of transducer frequencies (31.25 kHz to 4 MHz) [77]. The TDC7200 is a Time to Digital Converter (TDC) that performs the function of a

stopwatch. It is used to measure time between a single event (edge on START pin) and multiple subsequent events (edges on STOP pin). The device has an internal self-calibrated time base that is used to measure time with resolution in the order of 55 ps. Self-calibration compensates for drift over time and temperature and enables time-to-digital conversion accuracy in the order of picoseconds [78]. The TDC7200 has two measurement modes: Measurement Mode 1 and Measurement Mode 2. The choice of mode is to be based on the duration of time to be measured by the device [79].

a) In measurement mode 1 as shown in Figure 2.4, the TDC7200 performs the entire counting from START to the last STOP using its internal ring oscillator plus coarse counter. This method is recommended for measuring shorter time durations of <500 ns. Using measurement mode 1 for measuring >500 ns decreases accuracy of the measurement. The minimum time measurable in measurement mode 1 is 12ns.

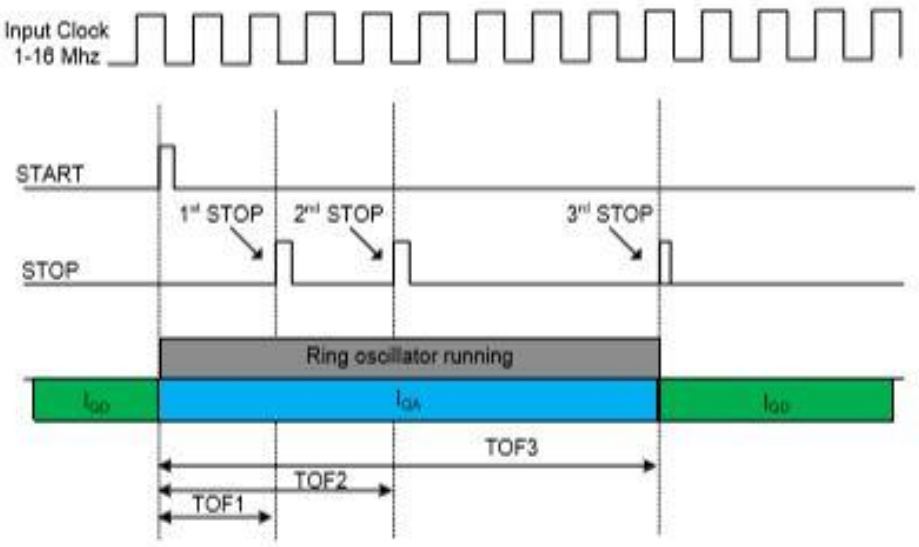

Figure 2.4: Measurement Mode 1 for the TDC7200 [79].

b) In measurement mode 2 as shown in Figure 2.5, the internal ring oscillator of the TDC7200 is used only to count fractional parts of the total measured time. The internal ring oscillator starts counting from when it receives the START signal until the first rising edge of the CLOCK. Then, the internal ring oscillator switches off, and the Clock counter starts counting the clock cycles of the external CLOCK input until a STOP pulse is received. The internal ring oscillator again starts counting from the STOP signal until the next rising edge of the CLOCK. This method is recommended for measuring long time durations and can only be used when the time between START and STOP is a minimum of two cycles of the external CLOCK. Since, TDC7200 device has a maximum clock frequency of 16 MHz, the minimum time measurable in mode 2 is 125 ns.

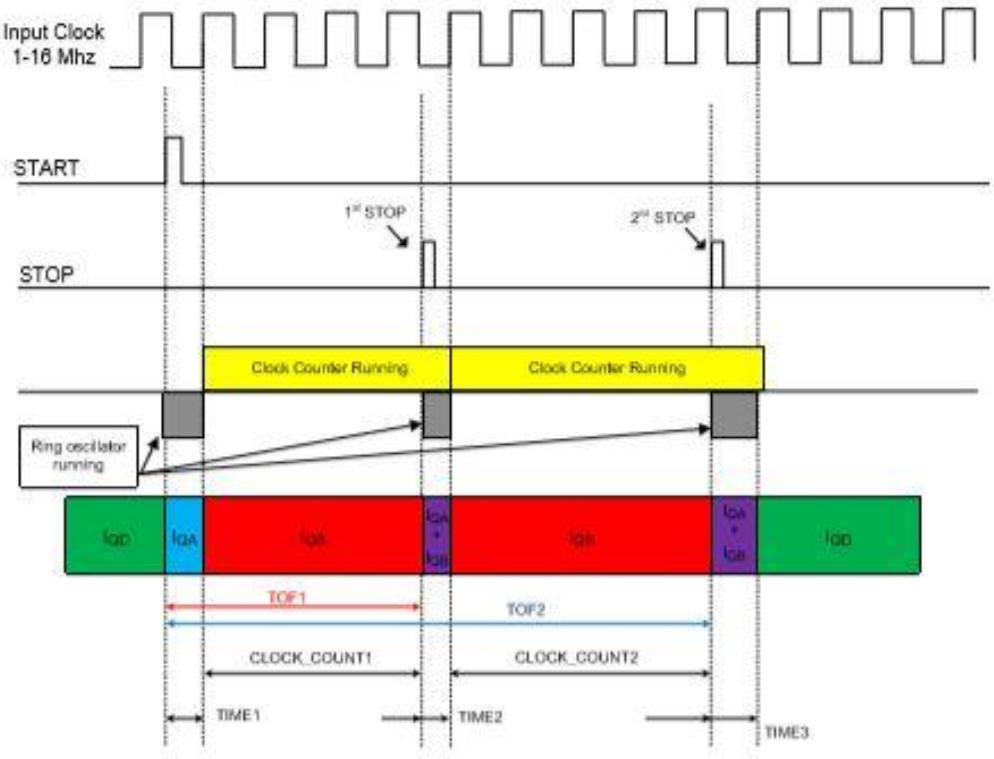

Figure 2.5: Measurement Mode 2 for the TDC7200 [79].

(b) Arduino Uno Rev3

The Arduino (shown in Figure 2.6) is a microcontroller board based on the ATmega328P that constitutes several digital pins that can act as either inputs or outputs. It has 14 digital input/output pins (of which 6 can be used as PWM outputs), 6 analog inputs, a 16 MHz quartz crystal, a USB connection, a power jack, an ICSP header and a reset button. The microcontroller has a clock speed of 16 MHz and has a recommended input voltage range of 7 – 12 V [80]. The board can be powered using a USB connection or can be directly connected to the power supply using appropriate power jack. This board is available for less than 25 USD and can be used for multiple applications. The 40 kHz HC-SR04 sensors can be used exclusively with the Arduino Uno. The availability of various online repositories allows users to easily program the device to suit multiple application. The Arduino can be programmed using the Arduino Integrated Development Environment (IDE).

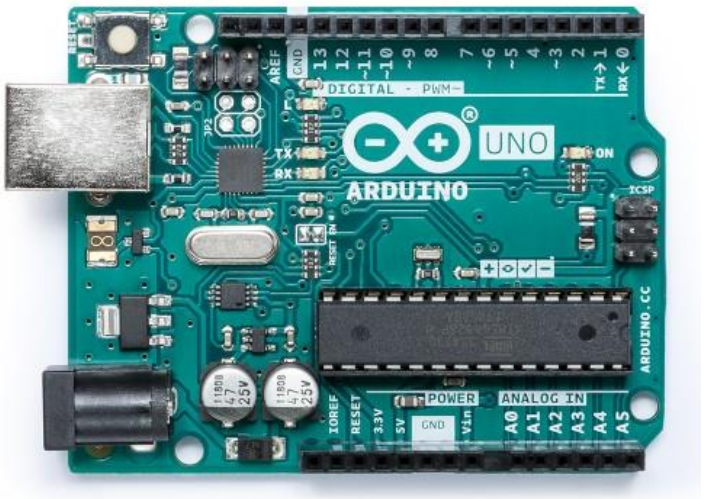

Figure 2.6: Arduino Uno R3 (Source: store.arduino.cc).

2.2 Benchtop Electronics

The Benchtop equipment used in the laboratory is Function generator and Oscilloscope. The Function generator is used to power the ultrasound transmitter. The transmitter is powered using a continuous series of eight bursts with frequencies of 1 MHz and a delay of about 600 µs to ensure that the waveforms from the ultrasound receiver are read properly. The signals of both the ultrasound transmitter and the receiver are observed with the help of an Oscilloscope. The specifications of the benchtop electronics are as follows:

2.2.1 Function Generator

GW INSTEK AFG-2225 is a basic level dual-channel arbitrary function generator where both the channels are equipped with same characteristics to fit dual-signal applications such as differential signalling [81]. The features of this function generator include:

- Wide frequency ranges from 1µHz to 25MHz (sine/square wave)
- 1 µHz Resolution in full range
- Built-in standard 120MSa/s, 10bit, 4k points arbitrary waveform for both channels
- True Dual-Channel output, Channel two provides the same characteristics as Channel one
- Couple, Tracking, Phase operations of dual channel are supported
- 1% ~ 99% adjustable duty cycle for square waveform
- High Resolution and Coloured TFT LCD with friendly user interface
- Built-in standard AM/FM/PM/FSK/SUM/Sweep/Burst and frequency counter
- USB Host/Device interface for remote control and waveform editing

The function generator is used to trigger the ultrasound sensor. The ultrasound sensor is triggered by providing continuous eight burst (or more) sinusoidal signal of a fixed voltage equal to 10 V_{pp} or according to the sensor configuration. Figure 2.7 depicts the Function Generator used in the lab.

Figure 2.7: Function generator used in the laboratory (Source: newark.com).

2.2.2 Oscilloscope

The Oscilloscope (KEYSIGHT Model: MSO-X 2024 A) is used to observe the signal coming from the function generator and the signal from the ultrasound receiver. The Oscilloscope used in the laboratory (as shown in Figure 2.8) consists of four channels with 70 MHz bandwidth and a maximum sample rate of 2 GSa/s. It features an 8.5-inch display and has USB slots to save or load waveforms for further analysis. The oscilloscope also comes loaded with measurement features to analyse the waveform and measure the various waveform parameters [82].

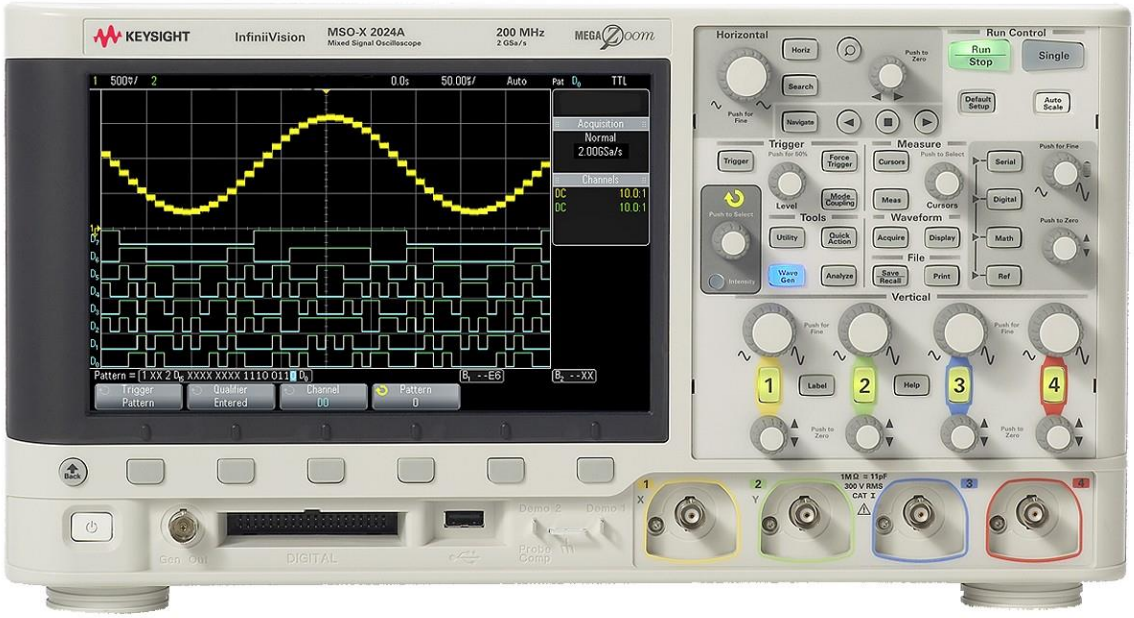

Figure 2.8: Oscilloscope used in the laboratory (Source: tequipment.net).

2.3 Chemicals and Bacterial Cells

The bacterial cells are cultivated on Difco™ Modified membrane - Thermotolerant *E. coli* Agar (modMTEC) (BD Diagnostics, Sparks, MD) plates by streaking these plates with RAS (Returned Reactivated Sludge) samples collected from Milwaukee Metropolitan Sewerage District (MMSD). The plates are created by first dissolving powdered Difco™ modMTEC in a liter of De-Ionized (DI) water in an autoclave safe beaker. The mixture is autoclaved at 121 °C for 30 minutes. The liquid is then poured into petri-dishes and allowed to solidify. The culture dishes are then stored in 4 °C refrigerator.

The modMTEC plates are streaked with RAS using a blue loop and following streaking techniques. These plates were then kept in the incubator at 35°C for 2 hours followed by 22 hours

at 44.5 °C [83]. One bacterial colony, indicated by purple dots (as shown in Figure 2.9), was picked and inoculated with 5 mL of Lysogeny Broth (LB) media (prepared by suspending 10 g tryptone, 5 g yeast extract and 10 g common salt in 1 L of DI water and autoclaved at 121 ºC. After cooling down, the flask is swirled to ensure mixing [94[) which is a favorable nutrient for *E. coli* to grow and left in the incubator for 24 hours at 37 °C, shaking at 100 rpm on an OrbiShaker™ MP Micro plate Shaker (Benchmark Scientific, Inc., Edison, NJ).

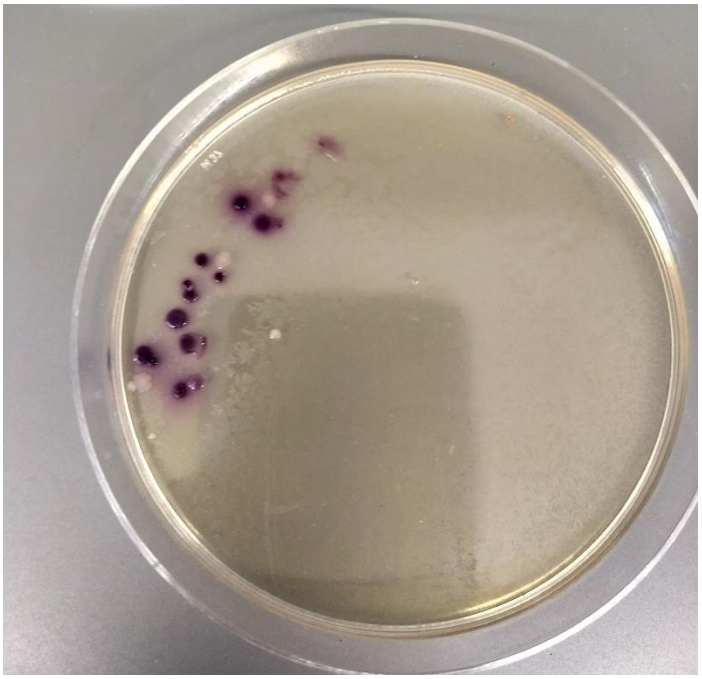

Figure 2.9: The presence of *E. coli* is indicated by the purple dots on the culture dish. The purple dots are visible after streaking the plates with RAS and stored in the incubator at 44.5 °C for 24 hours.

These prepared samples were then stored in 4 °C refrigerator (for use within seven days from the date of preparation). Biofilm is then grown by adding 5 mL of *E. coli* bacterial cells (prepared earlier) to 20 mL of LB media inside a plastic box (kept stationery inside the incubator) (as shown in Figure 2.10) for tests using the ultrasound sensor.

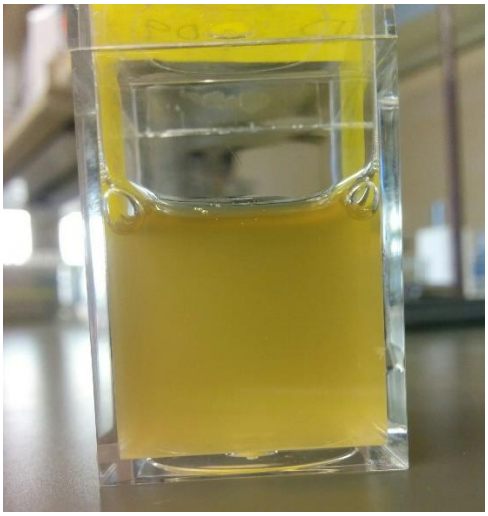

Figure 2.10: Plastic box in which biofilm of *E. coli* bacteria is grown. The diminished yellow color (or the liquid being opaque) represents the presence of biofilm in the liquid. On the first day, the liquid is transparent.

Agar based gel was solidified by adding water to the powder substance and then boiling it such that the yellow powder completely dissolved in the boiling water. A microscope slide is then dipped into the beaker with the aqueous gel and then cooled by drying it out in air. Another substance used to simulate the presence of biofilm is PolyHEMA, since it is a soft, flexible, water-absorbing plastic used to make soft contact lenses. A 95% ethanol solution was prepared by dissolving 50 mL of DI water in 950 mL of denatured (A-407) ethyl alcohol (Fisher Scientific, NJ) solution. Different concentrations of the PolyHEMA crystal (Sigma-Aldrich, G9012-100ML) was dissolved in 2 mL of 95% ethanol on the cap of a bottle (as shown in Figure 2.11). The PolyHEMA was left to solidify by leaving them inverted, inside the incubator (set to 35 °C) overnight.

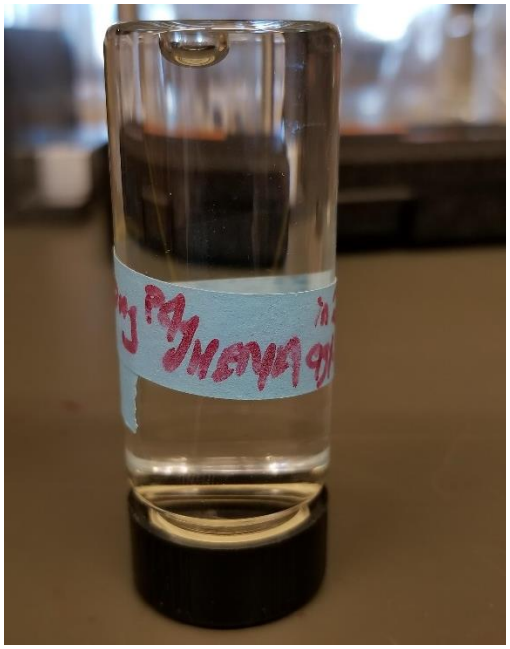

Figure 2.11: PolyHEMA coating on the cap of a bottle for facilitating the measurement of thickness. A white coating can be observed on the cap of the bottle. This coating represents the solidified PolyHEMA.

Sample tests are performed using DI water and plain tap water. These tests were used as a control (or reference) for the test with biofilm, PolyHEMA and other objects readily available in the laboratory.

2.4 Miscellaneous Materials

Materials that are readily available in the laboratory is used as test objects to successfully test the proof of concept. These materials include aluminum foil, paper towels, Ziploc® bags, A4-sized print papers, nitrile-free hand gloves and a combination of the materials listed here. Spectra ultrasound gel was used as a couplant for the sensors to facilitate the transmission of ultrasound into the test chambers. This is necessary to reduce the interference from air on the sensor reading.

Chapter 3

Experimental Methods

The experiments were performed in stages as preliminary steps to ensure that the concept developed in the laboratory can be used for the detection of biofilm. These different steps are listed in the following sections. The data from different trials of the biofilm, PolyHEMA and solubility experiment were analyzed using boxplot generated using MathWorks MATLAB and the Pearson correlation factors were determined using the SYSTAT SigmaPlot.

3.1 Experiment using Arduino

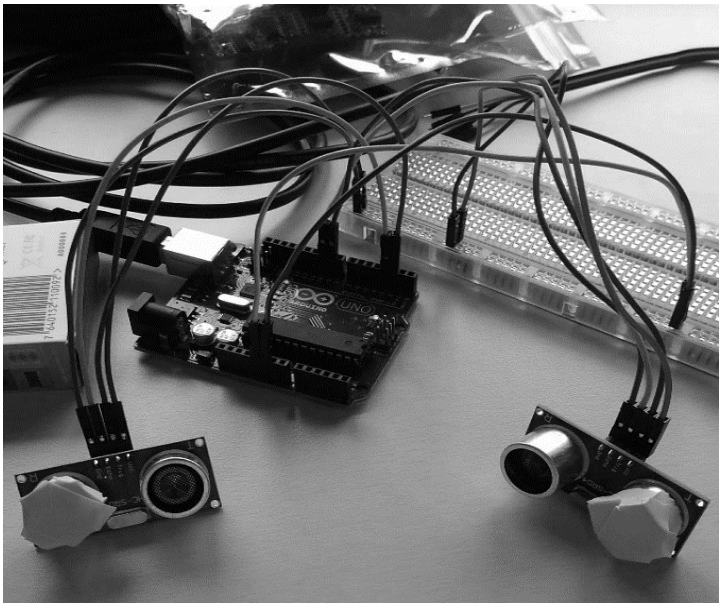

Figure 3.1: Experiment setup using Arduino Uno and HC-SR04 sensor. The receiver of one HC-SR04 and transmitter of the other sensor has been taped to avoid interference from these signals in the output sensor data.

Arduino Uno was used as an evaluation board in this experiment. Arduino custom sensors (HC-SR04) were used to detect any test objects. A code (shown in Appendix A) was developed

for the Arduino Uno so that it can trigger one sensor and then receive the echo signal through a second sensor. This test arrangement can be seen in Figure 3.1. The receiver of one HC-SR04 and the transmitter of the other HC-SR04 was sealed using electrical tapes to avoid interference between signals. The output of the sensors was recorded to an Excel file using custom software (as shown in Figure 3.2, details in Appendix B) that was developed in the laboratory.

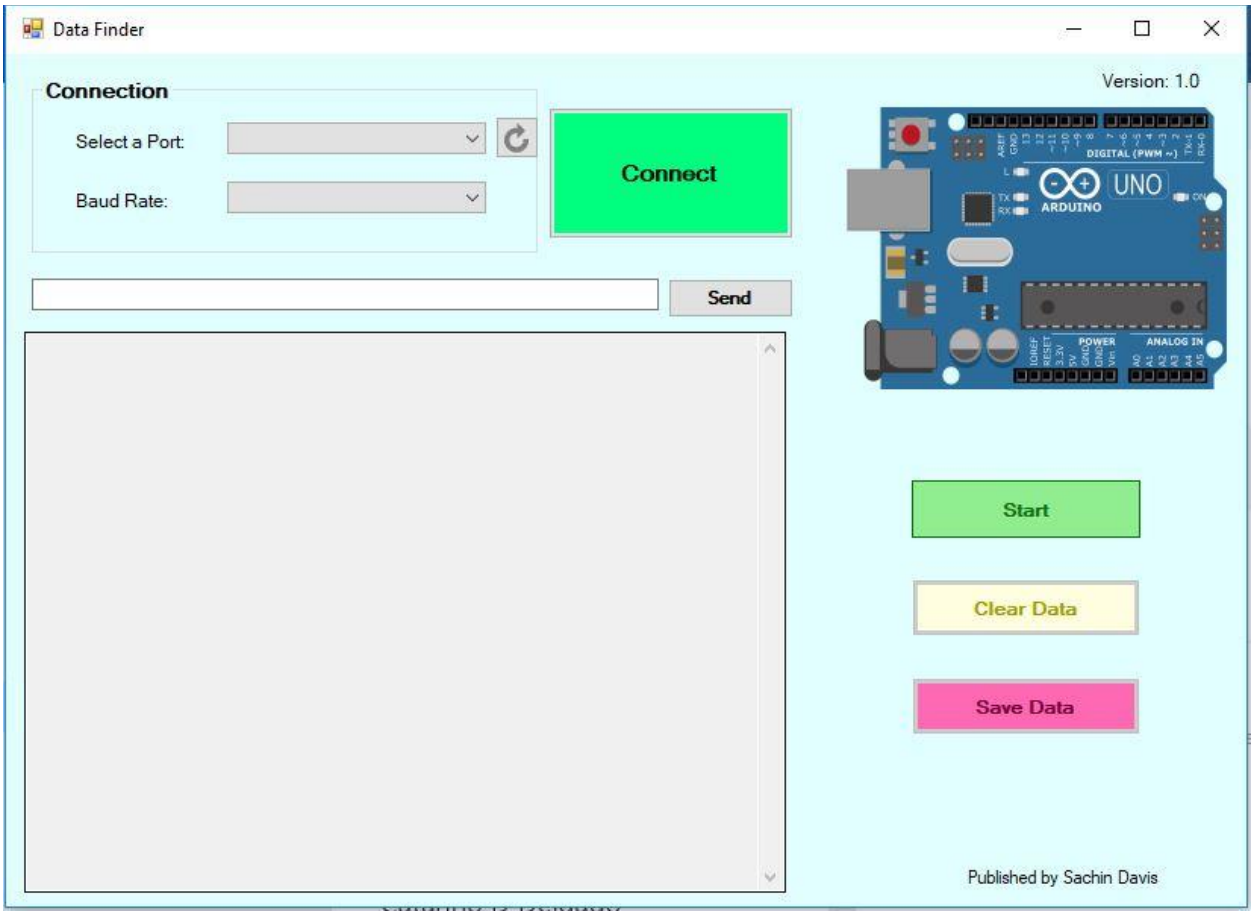

Figure 3.2: Software (screen interface) used to extract data from the Arduino sensors. The software provides interface to enable communication between the software and Arduino Uno. The 'Save Data' button saves the data on the serial monitor to an excel file.

The experiment with the Arduino Uno was performed with two mediums – air and water. When air was used as the medium, the procedures for the experiment is listed below:

a) One HC-SR04 sensor was placed on a side of the platform on which measurement is to be performed. This sensor is treated as the transmitter sensor. Since the HC-SR04 sensor consists of a transmitter and receiver, the receiver sensor is taped so that this sensor does not receive any signal.
b) The other HC-SR04 sensor was placed on the other side of the platform. This sensor is treated as the receiver sensor and the transmitter sensor of this HC-SR04 module is taped so that this sensor does not emit any signal.
c) The trigger pin of both the transmitter and the receiver sensor is connected to a digital pin of the Arduino which goes high and low to mimic an edge triggered signal to activate the ultrasound sensors.
d) The echo pin of the receiver sensor is connected to an Arduino digital pin which waits for the receiver signal.
e) Both the transmitter and the receiver sensors are connected to the 5 V power and ground output pins of the Arduino
f) Measurements were taken for two different instances – one with no test object present in the path between the two sensor and the other when a test object (cardboard box, plain paper) were placed on the path between the two ultrasound sensors.
g) Using the software developed in the laboratory (as shown in Figure 3.2), the readings of the receiver sensor were recorded and saved to an excel file for future analysis.

When water was used as a medium, the experiment using Arduino was performed using the following procedure:

a) One HC-SR04 sensor was placed on the side of the platform, filled with DI water to the brim, on which measurement is to be performed. This sensor is treated as the transmitter sensor. Since the HC-SR04 sensor consists of a transmitter and receiver, the receiver sensor is taped so that this sensor does not receive any signal.
b) The other HC-SR04 sensor was placed on the other side of the platform. This sensor is treated as the receiver sensor and the transmitter sensor of this HC-SR04 module is taped so that this sensor does not emit any signal.
c) The trigger pin of both the transmitter and the receiver sensor is connected to a digital pin of the Arduino which goes high and low to mimic an edge triggered signal to activate the ultrasound sensors.
d) The echo pin of the receiver sensor is connected to an Arduino digital pin which waits for the receiver signal.
e) Both the transmitter and the receiver sensors are connected to the 5 V power and ground output pins of the Arduino.
f) Measurements were taken for two different instances – one with no test object present in the path between the two sensor and the other when a test object (plastic box filled with cotton, paper napkins) were placed on the path between the two ultrasound sensors inside water.
g) Using the software developed in the laboratory (as shown in Figure 3.2), the readings of the receiver sensor were recorded and saved to an excel file for future analysis.

3.2 Experiment using a Function generator and Oscilloscope

The experiment using the Function generator and the Oscilloscope was performed using a plastic chamber which was designed in the laboratory and filled with DI water. The procedures followed for this experiment are listed below:

a) One, 1 MHz ultrasound sensor was placed on one side of the plastic chamber filled with DI water. This sensor is manufactured such that it can act as both transmitter and/or receiver. The sensor leads are connected to the function generator output so that it acts as an ultrasound transmitter.

b) A second ultrasound sensor is placed on the other side of the chamber such that, when the chamber is viewed from the side lengthwise, the sensors are placed in a straight line. The leads for the sensor are connected to the Oscilloscope so that it acts as an ultrasound receiver. The arrangement of the sensors can be seen in Figure 3.3.

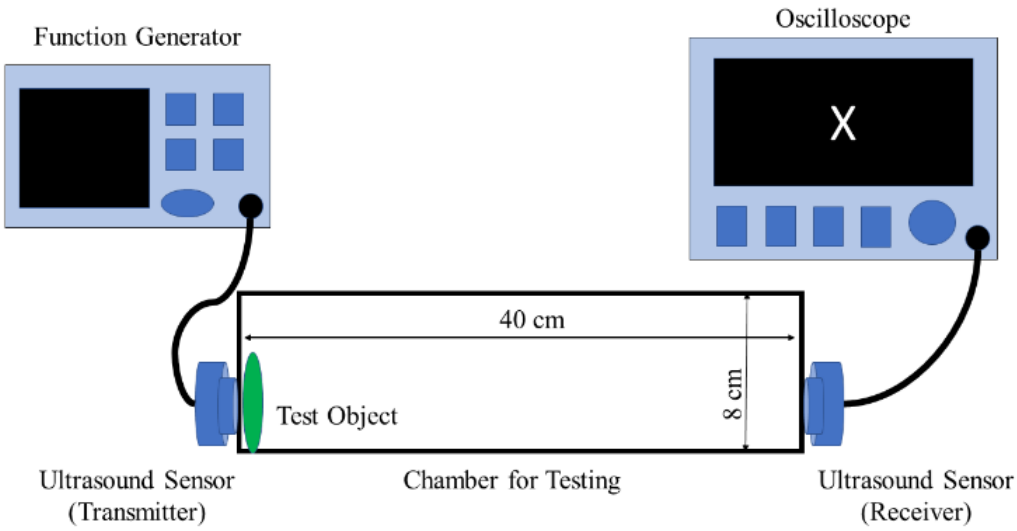

Figure 3.3: Schematic representation of the sensor arrangement. The sensors (transmitter sensor and receiver sensor) are placed on either side of the chamber. The transmitter and receiver sensors are connected to the function generator and the oscilloscope respectively.

c) The function generator settings are adjusted such that it produces a burst output. The burst output setting is selected such that the frequency generator sends a period eight-burst signal with a period of 10 ms and a delay of about 655 µs. The amplitude and frequency of the wave generated by the function generator is 10 V_{pp} and 1 MHz respectively. The function generator settings can be seen in Figure 3.4.

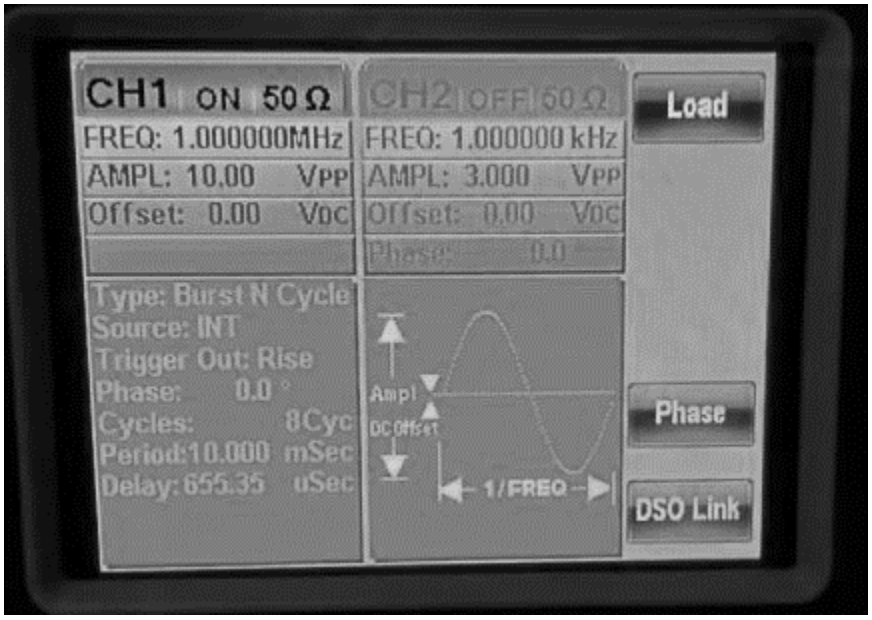

Figure 3.4: A screen showing the settings of the function generator that activates the 1 MHz ultrasound sensor. The output is generated from the first channel and it can be noted that this channel is on, while the other channel is off.

d) The output of the Function generator is also connected to one of the probes of the Oscilloscope so that the input to the transmitter sensor can be observed.

e) The voltage and phase shift parameters of the output data from the receiver sensor is recorded from the Oscilloscope screen and saved to an excel file for future analysis.

f) Different test objects were placed in water in the path between the sensors and the variations in the two parameters were recorded in excel files. The test objects used were

materials that are readily available in the laboratory like A4 paper, plastic Ziploc® bag, aluminium foil. The other test objects used were *E. coli* biofilm that was grown in plastic boxes over a period of several days and PolyHEMA grown in the caps of bottles using different concentrations of PolyHEMA in 95% ethanol solution.

3.3 Experiment using TDC board and Oscilloscope

The experiment using the TDC board was performed using the same plastic chamber as used in the previous experiment. The steps for this experiment are described below:

a) One, 1 MHz ultrasound sensor was placed on one side of the plastic chamber filled with DI water. This sensor is manufactured such that it can act as both transmitter and/or receiver. The sensor leads are connected to the TDC TX1 pin for transmitter sensor so that it acts as an ultrasound transmitter.

b) A second ultrasound sensor is placed on the other side of the chamber such that, when the chamber is viewed from the side lengthwise, the sensors are placed in a straight line. The leads for this sensor are connected to the TDC RX1 pin so that it acts as an ultrasound receiver. The arrangement of the sensors can be seen in Figure 3.3.

c) The TDC board settings can be adjusted such that measurement mode 2 setting is selected to enable activate the ultrasound transmitter to produce continuous bursts of signals and these signals are received using the ultrasound receiver. The receive mode setting of the TDC is set to Multi Echo to ensure that the evaluation board is looking for receiver sensor data. The continuous trigger setting is enabled so that continuous output can be observed on the Oscilloscope. A screenshot of the settings used in TDC evaluation software is shown in Figure 3.5.

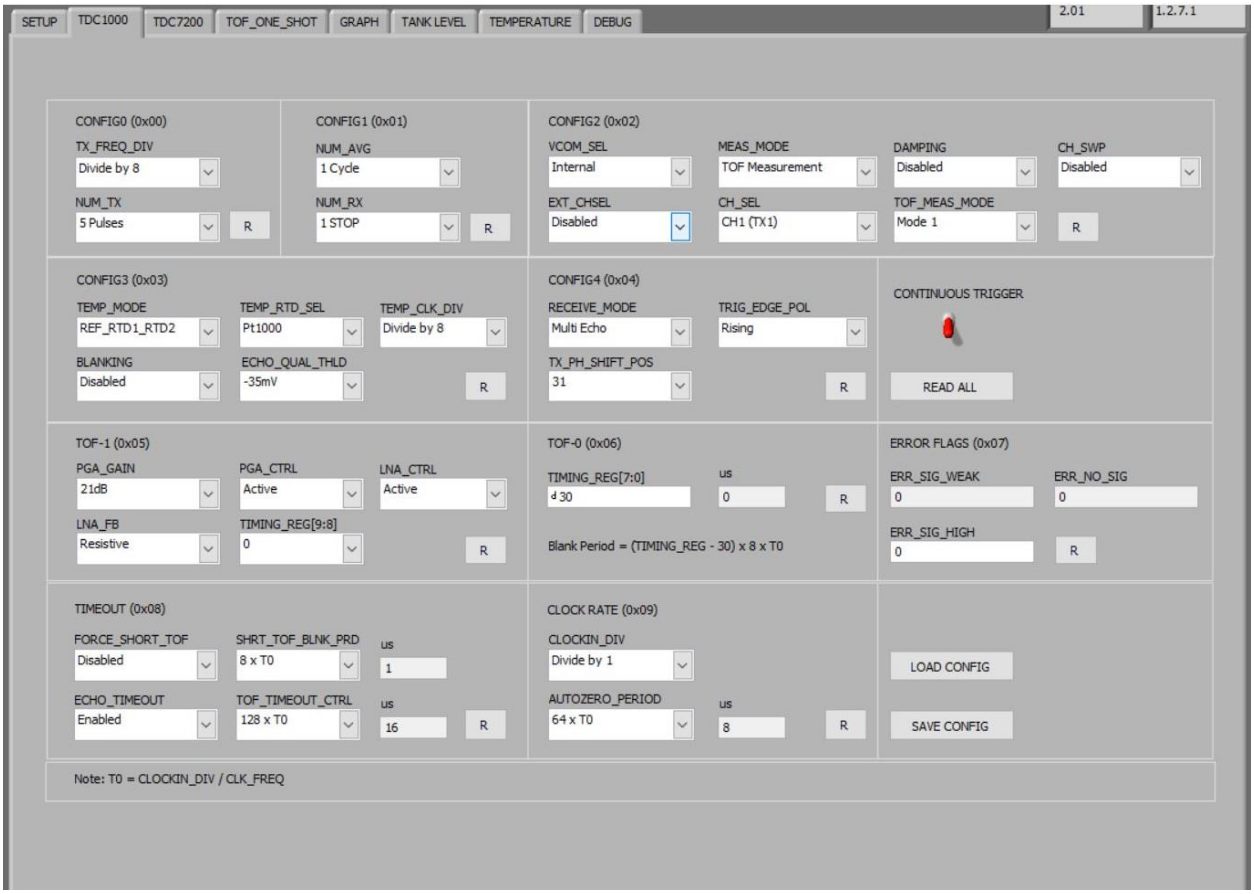

Figure 3.5: A screenshot depicting the TDC evaluation software. The settings used to activate the ultrasound sensor can be observed in this screenshot.

d) The Oscilloscope probes are connected to the START, STOP and COMP output of the TDC evaluation board to observe the transmitter input and the receiver data. The test setup can be seen in Figure 3.6.

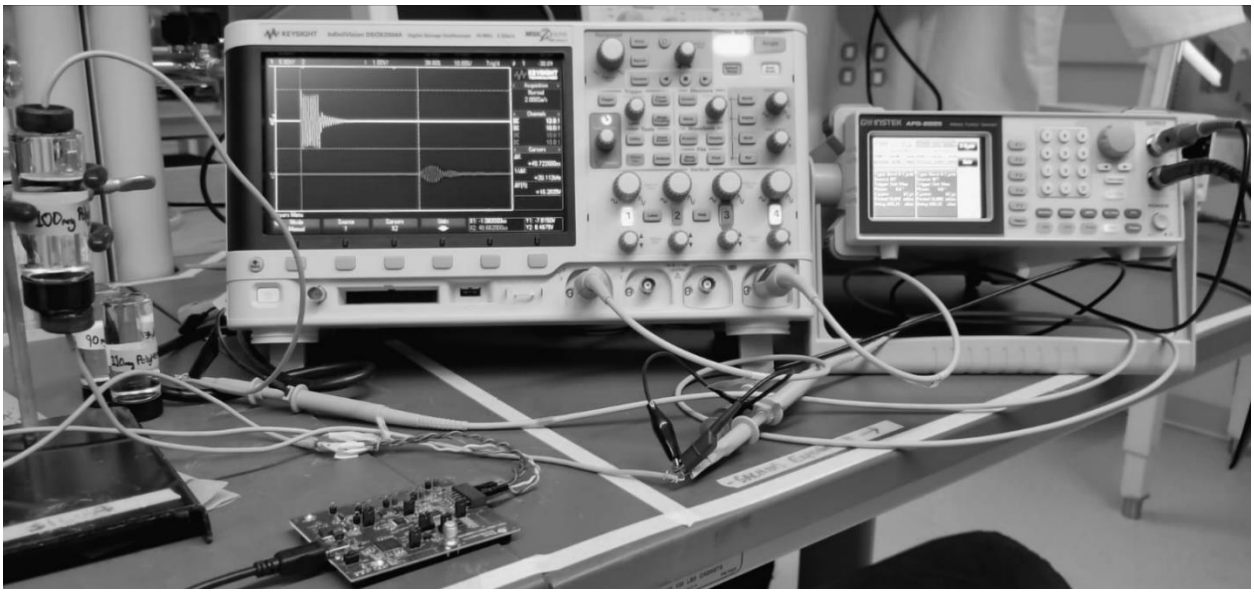

Figure 3.6: Test setup using the TDC board and Oscilloscope. A function generator is also shown in the background. The test setup can be used for measuring the growth of biofilm.

e) The voltage and phase shift of the received data was recorded from the Oscilloscope screen to an excel file for future analysis.

f) Different test objects were placed in water in the path between the sensors and the variations in the two parameters were recorded in excel files. The test objects used were materials that are readily available in the laboratory like A4 paper, plastic Ziploc® bag, aluminium foil. The other test objects used were *E. coli* biofilm that was grown in plastic boxes over a period of several days and PolyHEMA grown in the caps of bottles using different concentrations of PolyHEMA in 95% ethanol solution.

3.4 Experiment to determine the effect of solubility on sensor data

The experiment to determine the effect of solubility on sensor data was performed by using the procedures listed below:

a) One, 1 MHz ultrasound sensor was placed on one side of a plastic box filled partially with DI water. The sensor leads are connected to the function generator output so that it acts as an ultrasound transmitter.

b) A second ultrasound sensor is placed on the other side of the box such that the sensors are placed in a straight line. The leads for this sensor are connected to the Oscilloscope so that it acts as an ultrasound receiver. The arrangement of the sensors can be seen in Figure 3.7.

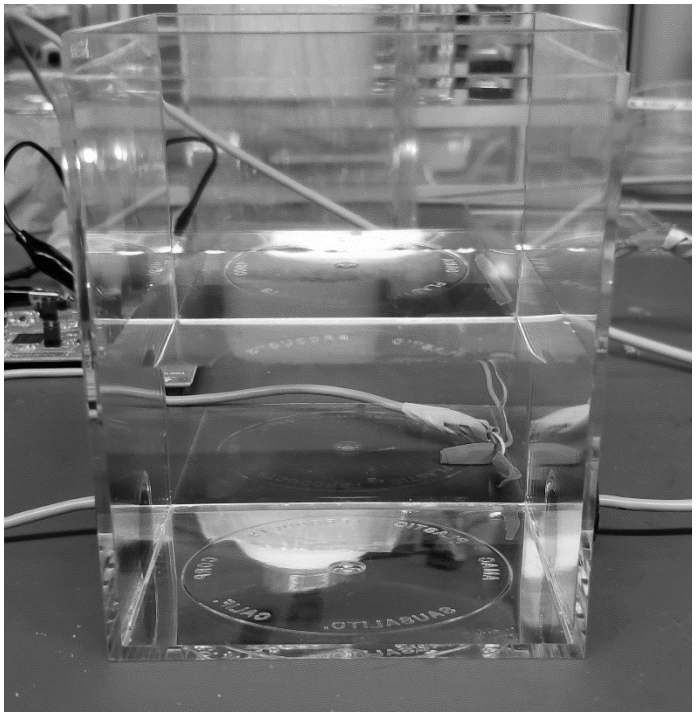

Figure 3.7: The experiment setup to determine the effect of solubility on sensor data. The ultrasound sensors are placed in a straight line on the opposite side of the plastic box.

c) The function generator settings are adjusted such that it produces a burst output. The burst output setting is selected such that the frequency generator sends a period eight-burst signal with a period of 10 ms and a delay of about 655 µs. The amplitude and frequency of the wave generated by the function generator is 10 V_{pp} and 1 MHz respectively. The function generator screen can be seen in Figure 3.4.

d) The output of the Function generator is also connected to one of the probes of the Oscilloscope so that the input to the transmitter sensor can be observed.

e) The voltage and phase shift parameters of the output data from the receiver sensor is recorded from the Oscilloscope screen and saved to an excel file for future analysis.

f) One gram of Morton's Iodized salt is slowly added to the plastic box with DI water and stirred continuously with the help of a smart spatula until no more salt can be added or the solution reaches saturation. The two parameters are recorded at each stage and recorded in an excel file.

3.5 Experiment to determine the effect of different materials on sensor data

The experiment to determine the effect of materials on sensor data was performed for two different material thickness – two inches and three inches and three different materials – Polyvinyl Chloride (PVC), Copper and Galvanized Iron. The procedure followed for recording sensor data is listed below:

a) One, 1 MHz ultrasound sensor was placed on one side of the two inches PVC piping chamber filled with tap water. The sensor leads are connected to the function generator output so that it acts as an ultrasound transmitter.

b) A second ultrasound sensor is placed on the other side of the piping chamber such that the sensors are placed in a straight line. The leads for this sensor are connected to the Oscilloscope so that it acts as an ultrasound receiver. The arrangement of the sensors can be seen in Figure 3.8.

c) The function generator settings are adjusted such that it produces a burst output. The burst output setting is selected such that the frequency generator sends a period eight-burst signal with a period of 10 ms and a delay of about 655 µs. The amplitude and frequency of the wave generated by the function generator is 10 V_{pp} and 1 MHz respectively. The function generator screen can be seen in Figure 3.4.

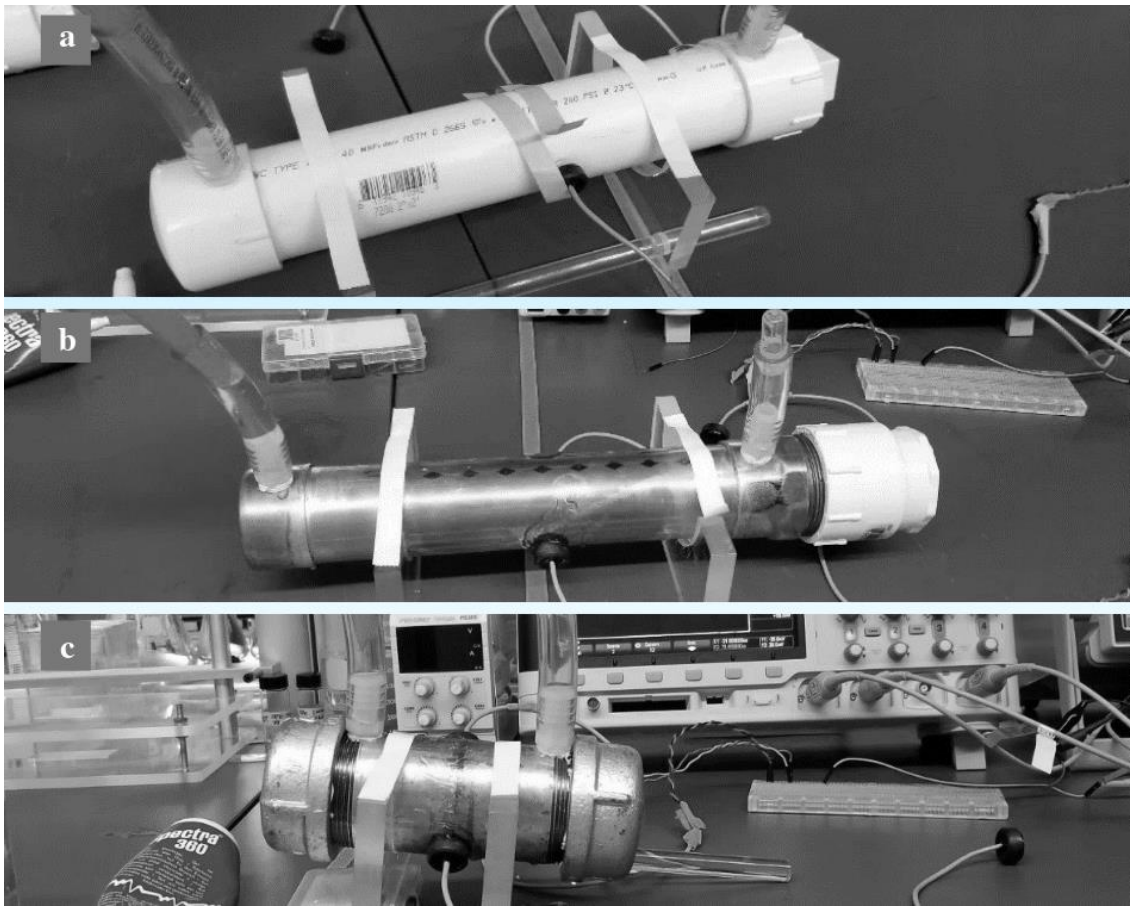

Figure 3.8: Two inches piping design with three different materials (a) PVC, (b) Copper and (c) Galvanized Iron. The sensors are placed on either side of the piping design.

d) The output of the Function generator is also connected to one of the probes of the Oscilloscope so that the input to the transmitter sensor can be observed.

e) The voltage and phase shift parameters of the output data from the receiver sensor is recorded from the Oscilloscope screen and saved to an excel file for future analysis.

f) The above steps are repeated for the two inches materials - Copper and Galvanized Iron and the sensor data is saved to an excel file.

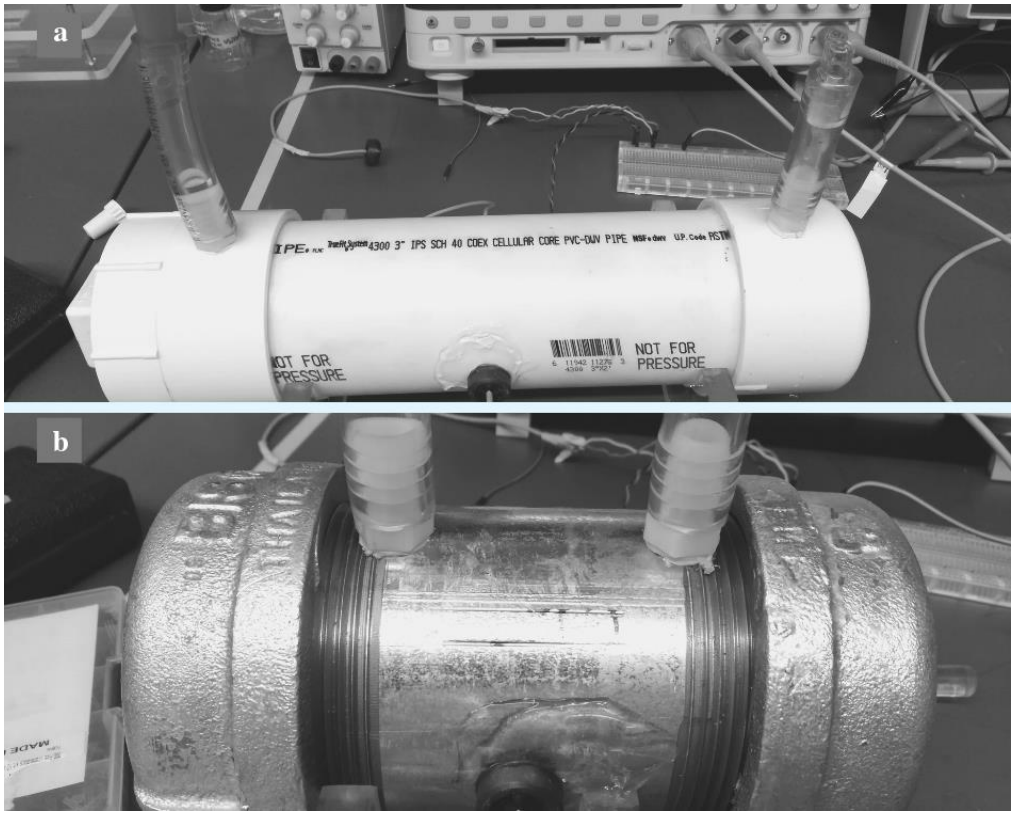

Figure 3.9: Three inches piping design with two different materials (a) PVC, and (b) Galvanized Iron. The sensors are placed on either side of the piping design.

g) For three inches – PVC and Galvanized Iron, steps a – e, are repeated, and the sensor data is saved in an excel file. Three inches Copper material was not tested since they are not used in either household or industrial piping systems.

Chapter 4

Results and Discussion

The idea behind the use of ultrasound sensor arrangement (discussed in the research) in a closed system is best described in Figure 4.1. When the closed piping system is devoid of biofilm presence and the sensors are placed on opposite sides of the sensor, then the receiver sensor will display a voltage which has amplitude lower than that of the transmitted voltage. When there is a contaminant presence (or biofilm presence) on the inner walls of the closed pipe system, then the detected voltage is both shifted in phase and the voltage level is attenuated (as seen in Figure 4.1).

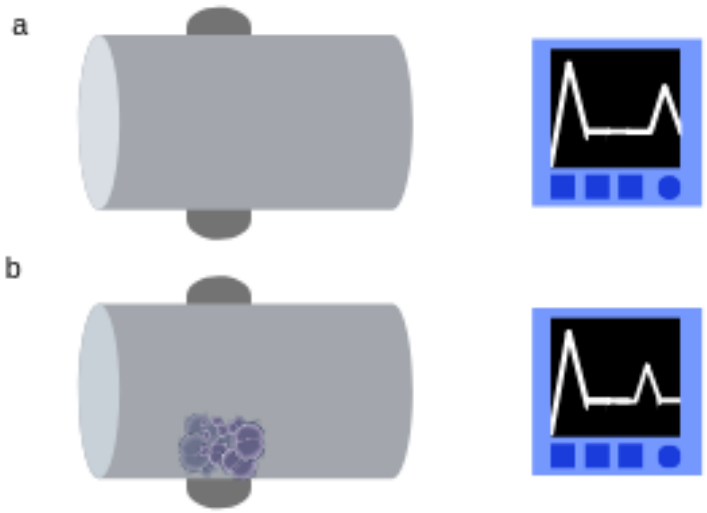

Figure 4.1: A schematic indicating the sensor arrangement and the method of detection of presence of contaminants. The first peak shown in the oscilloscope screen is the transmitter voltage peak while the second peak is the receiver voltage peak. (a) The sensors are placed on the outer wall of the closed system, the oscilloscope screen depicted next to it shows the voltage level observed. (b) When the closed system has presence of biofilm on its inner wall, the oscilloscope screen shows the receiver sensor data which is shifted by phase and the voltage level is attenuated.

4.1 Results of the experiments using Arduino

The Arduino experiment consists of the Uno board and an HC-SR04 ultrasound sensor. The ultrasound sensors were placed on either side of a test object and on either side of a test chamber filled with water. When air is the medium (as shown in Figure 4.2 i.e. the sensors are fixed facing each other such that the transmitter sensor of one HC-SR04 aligns with the receiver sensor of the other HC-SR04) the Arduino serial monitor reads a low value proportional to the distance of the test object from the sensor and when a test object is placed in the way of the two sensors (as shown in Figure 4.3), this value changes to a large value.

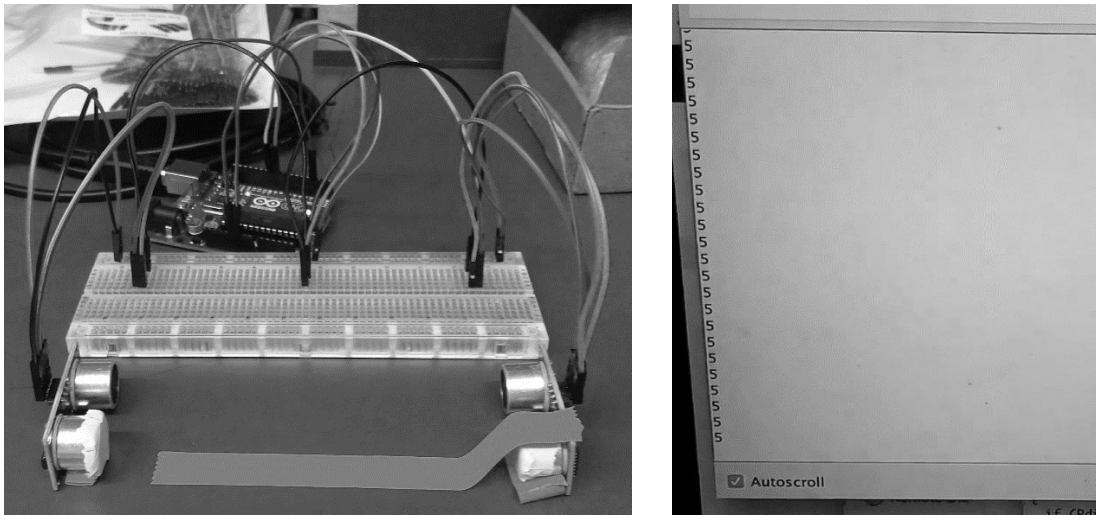

Figure 5.2: Arduino experiment setup with air as medium (left) and the serial monitor data (right) when there is no test object in the way of the sensors.

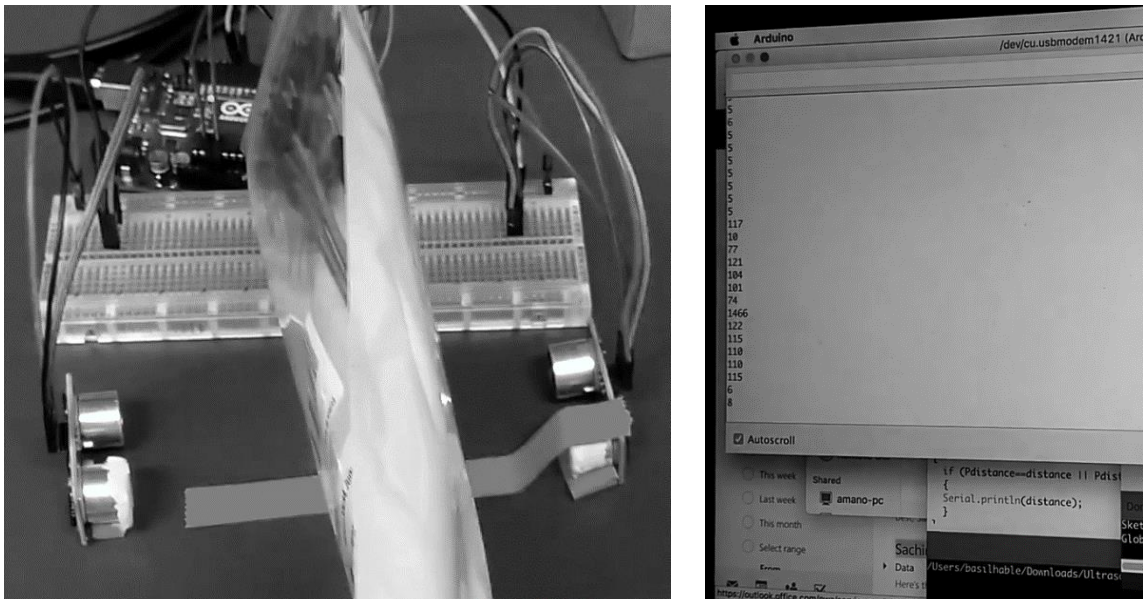

Figure 4.3: Arduino experiment setup with air as medium (left) and serial monitor data (right) when the test object is placed in the way of the two ultrasound sensors.

When water is used as the medium and the sensors are arranged (as shown in Figure 4.4) the results vary slightly. When there is no test object, the average value of the sensor data is lower than that when a test object is present inside the plastic chamber. In the Figure 4.4 below, the test object is nitrile-free gloves since it is readily available in the laboratory. When there is no test object, the average serial monitor data observed is around 16.5 cm and when the test object is placed inside the system, this value increases to about 18 cm (observed in Figure 4.5). However, these values were inconsistent, and this method cannot be used to detect biofilm.

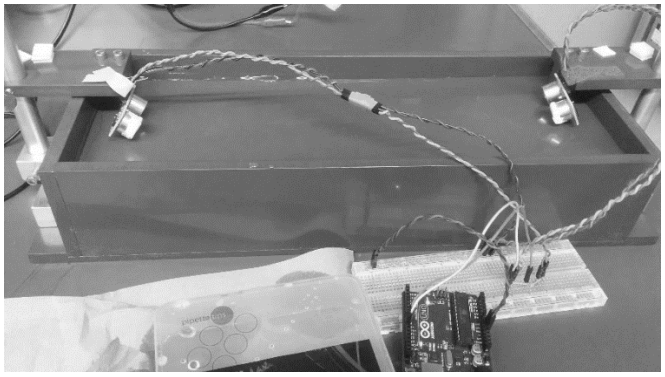

Figure 4.4: Arduino experiment setup. The plastic chamber is filled with water.

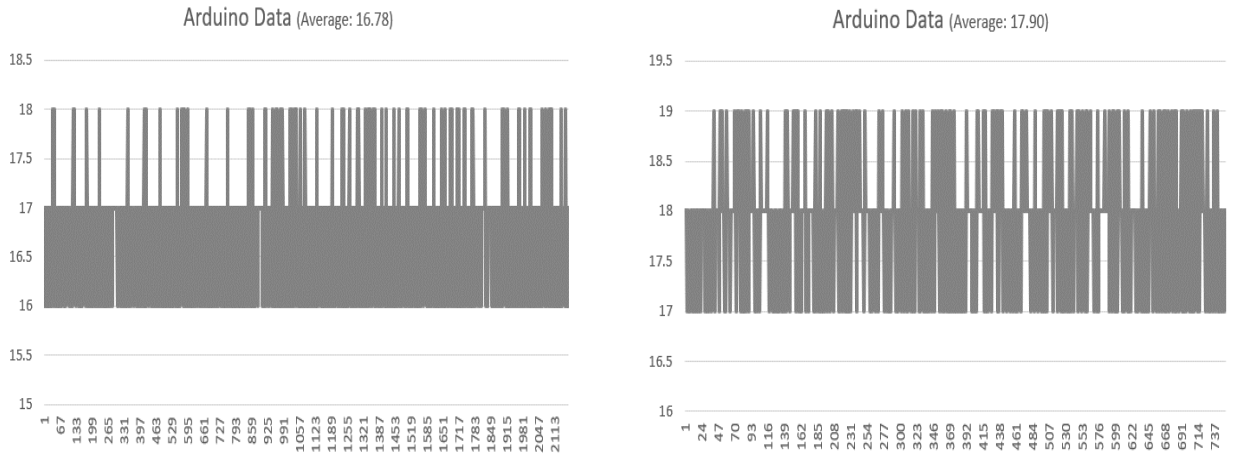

Figure 4.5: Serial monitor data observed with no test object (left) and when the test object is present (right).

The frequency of the HC-SR04 sensor is low and can only be powered by a 5 V supply. This signal is highly attenuated and is not suitable for our application as the attenuation of ultrasound in a channel with water as medium is more than that with solid as a medium.

4.2 Results of the experiments using Function generator/TDC board

A proof of concept experiment was successfully completed using the function generator and the oscilloscope. Test objects readily available in the laboratory were used to accomplish this task. The thickness of the test objects was measured with a micro-meter (Dicfeos, DM-09). The sensors were placed on either side of the plastic chamber filled with water (setup shown in Figure 4.6) and different test objects were inserted, in the way of the sensors, one by one and the results were recorded in Table 5. As the thickness of the test object used increases, the oscilloscope voltage decreases However, the current sensor arrangement is unable to detect objects with thickness less than 40 µm. This trend can be observed in Table 5, where the measured voltage remained the same when a halved Ziploc® (thickness of 22 micron) and a flat sheet of Aluminium foil (thickness of 16 micron) was introduced as a test object.

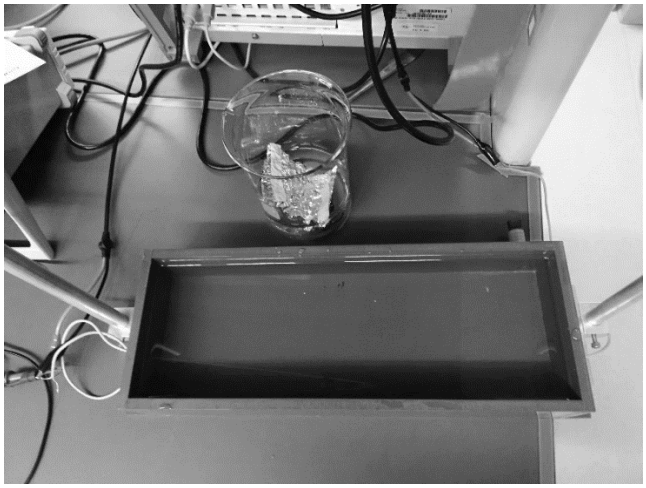

Figure 4.6: Proof of concept experiment setup

Table 5: Results of the proof of concept experiment. The test objects were chosen because of their easy availability in the laboratory.

Test Object	Thickness (mm)	Oscilloscope Voltage (mV)
No Test Object	0	63.3
Ziploc® Bag (Halved, i.e. Cut in half)	22	63.3
Ziploc® Bag	44	30
A4-sized Paper	50	30.3
Household Aluminum Foil	16	61.2

Following the success of the proof of concept experiment using the function generator, experiments were conducted with microscopic slides coated with different concentrations of agar-based gel. The results of this experiment can be seen in Table 6. The Pearson correlation of the agar experiment indicated a weak positive relationship (with a coefficient value of 0.14). This is because the settings of the evaluation were altered to avoid saturation of voltage. However, the trend remained the same for both trials of the experiment, where the voltage and phase data increased with an increase in the thickness of pure agar gel (which served as a good conductor of sound, amplifying the voltage levels).

Table 6: Results of the agar experiment. The data is comprised of change in Phase shift and Voltage change.

Test Object	Thickness	Max. Oscilloscope Voltage (V)	Phase Shift (μs)
No Test Object	0 μm	2.30	0.00
Microscope Slide	1 mm	1.32	-5.00
Agar-1.5% agar	1.050 mm 25 μm on each side	2.36	-2.50
Agar-2% agar 2 coat	1.300 mm 150 μm on each side	2.40	-3.75
Agar-2% agar 1 coat	1.060 mm 30 μm on each side	2.46	-2.25
No Test Object (new setting)	0 μm	1.30	0.00
Agar-1.5% agar (new setting)	1.050 mm 25 μm on each side	1.80	-2.50
Agar-2% agar 3 coat (new setting)	1.400 mm 200 μm on each side	1.90	-3.75
Agar-2% agar 1 coat (new setting)	1.060 mm 30 μm on each side	1.38	-2.50

An aqueous agar background does not change size or shape significantly even though the dry-weight agar concentration of the inclusion material differs from that of its surroundings It has been observed in the laboratory of Madsen and others [92]. This geometric stability does not exist for gelatin inclusions in gelatin surroundings, i.e., if the initial dry-weight gelatin concentration in the inclusion is greater than or less than that in the surroundings, the inclusion will increase or decrease in volume, respectively, presumably due to osmosis. Thus, for an aqueous mixture of agar and gelatin, a reasonable expectation is that the shape and size of inclusions will not change if the dry-weight gelatin concentration is the same in the inclusions as in the surroundings, while the dry-weight agar concentration in inclusions can be different than in the surroundings [92]. Agar-agar is insoluble in cold water, but it swells considerably, absorbing as much as twenty times

its own weight of water. It dissolves readily in boiling water and sets to a firm gel at concentrations as low as 0.50%. [93]. Agar coated glass microscope slide had similar attenuation properties to that of water since agar-based gel has a high amount of water present in it. By placing the microscope slide closer to the transmitter sensor, it increased the amount of transmitted wave and had less sound reflection. In the laboratory of Madsen et. al., the test corresponds to the doping of phantom particles along with the agar based-gel which helped them characterise the materials under the microscope. Similarly, biofilms are heavily saturated with EPS and other contaminants which makes the detection of the biofilm easier with the ultrasound sensor arrangement.

The sensors were then placed on either side of the plastic box containing biofilm (5 mL of bacterial cells added to 20 mL of LB media) and the sensors were triggered using the function generator and output was recorded using the oscilloscope. The results of a single trial can be seen in Table 7. The graphical view of the above table (Table 7) is shown in Figure 4.7 The graphical view gives a clear picture of the change in the different measured parameters much better than the tabular view. Figure 4.8 shows the graphical view of the results of the biofilm experiment for multiple trials. When repeating the experiment multiple times, the trend remains the same and the voltage and the phase measured decreases as the day of the experiment progresses.

Table 7: Results of a single trial of the biofilm experiment. The sensor data was recorded consecutively for eight days. The data is comprised of change in Phase shift and Voltage change.

Day	Function Generator Phase Shift Change (ns)	Function Generator Change in Voltage (V)	TDC Phase Shift Change (ns)	TDC Change in Voltage (V)
1	0.00	0.000	0.00	0.000
2	-55.00	-0.130	545.00	-0.196
3	-55.00	2.180	364.00	0.301
4	-55.00	1.240	182.00	0.470
5	-55.00	0.840	182.00	0.228
6	-691.00	3.740	0.00	-0.063
7	-411.00	3.640	1625.00	0.620
8	-379.00	2.840	433.80	0.540

The Pearson-correlation data for the biofilm experiment for multiple trials are recorded in Table 8. There is a strong relationship between the data (voltage, TDC voltage, phase and TDC phase) which indicates that both the voltage and the phase measured from the function generator can detect the presence of biofilms in piping system (or biofilm in plastic box in this case).

Table 8: Pearson-correlation data for the biofilm. A strong relationship exists when the Pearson correlation index is between 0.7 and 1. '*' indicates moderate or weak relationship or correlation of data between trials.

	Trial 1	Trial 2	Trial 3	Trial 4
Voltage (V)	1.00	0.80	0.88	0.50*
TDC Voltage (V)	1.00	0.92	0.85	0.88
Phase (µs)	1.00	0.94	0.98	0.90
TDC Phase (µs)	1.00	0.50*	0.06*	0.17*

a.

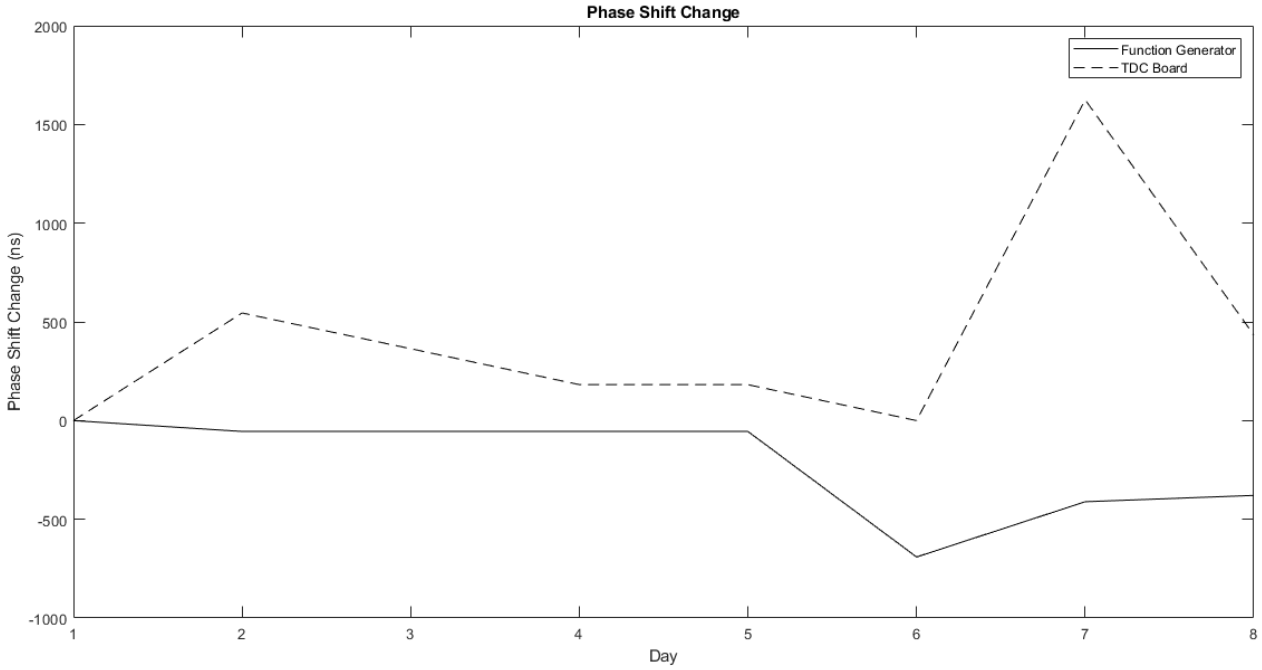

b.

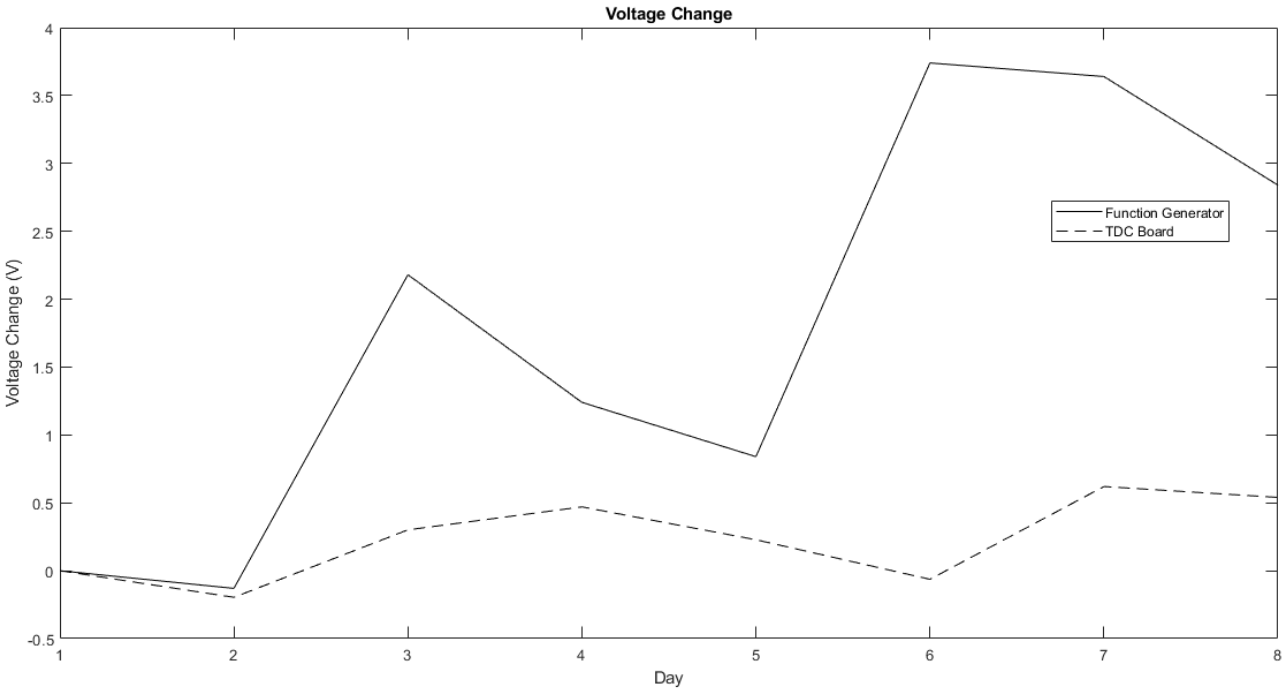

Figure 4.7: (a) Graph showing the variations in the phase change from day 1 to day 8. The phase variations are in the nanosecond range. (b) Graph showing the variations in the voltage change from day 1 to day 8. The bold line represents the measurements when the sensors are powered by the Function generator whereas the dashed line are those when the sensors are powered by the TDC evaluation board.

a.

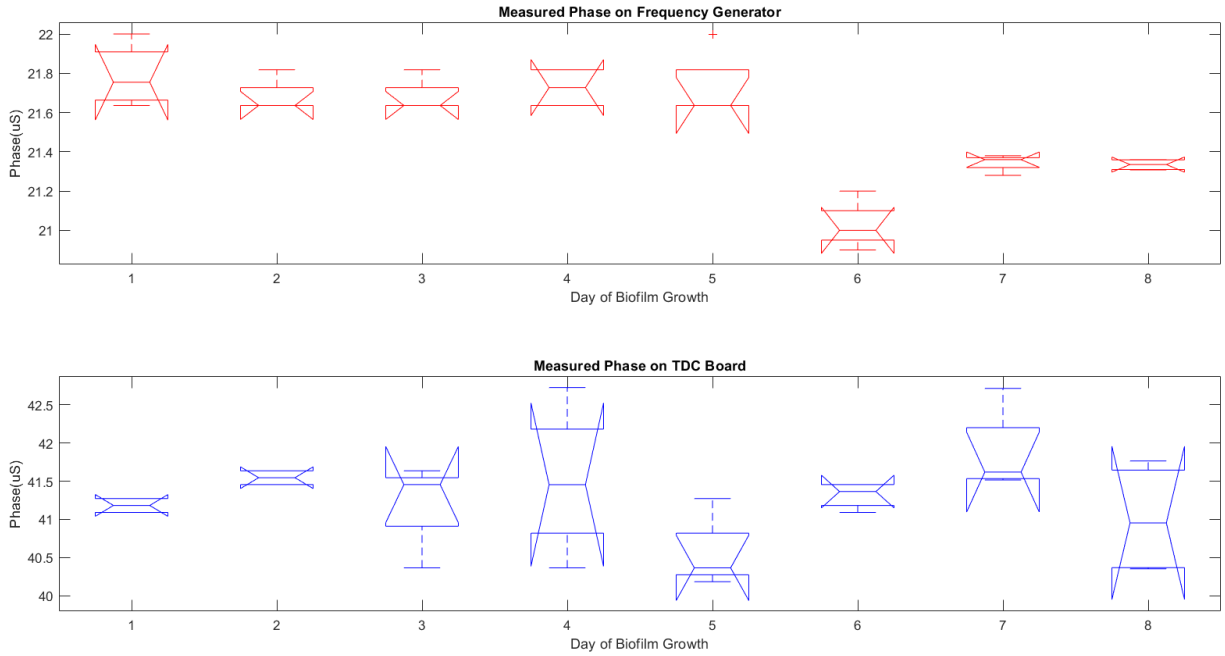

b.

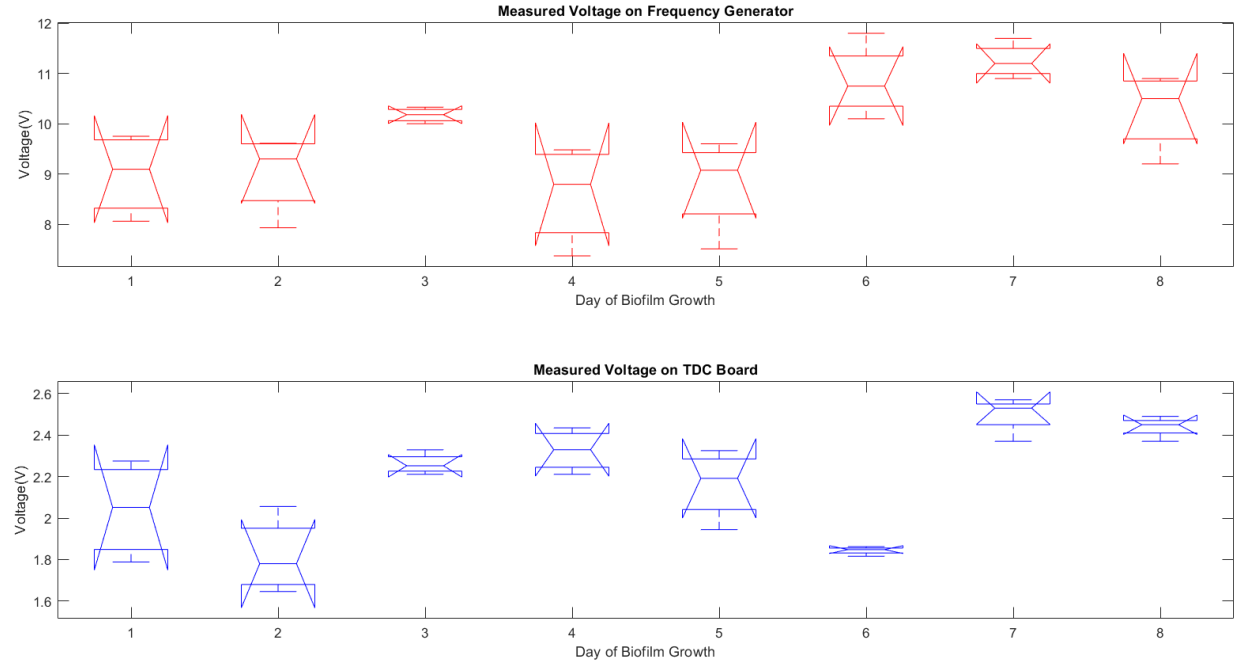

Figure 4.8: (a) Graph showing the analysis for variations in the phase change from day 1 to day 8 for four trials each. The phase variations are in the micro-second range. (b) Graph showing the analysis for variations in the voltage change from day 1 to day 8 for four trials each. The red trace represents the measurements when the sensors are powered by the Function generator whereas the blue trace represents the data of the sensors when they are powered by the TDC evaluation board.

The PolyHEMA experiment is set up like the biofilm experiment. The caps are left inside the incubator overnight (at 35 ºC) and the readings for thickness were obtained from the micrometer. The change in data was measured by taking the difference of measurements with plain DI water and PolyHEMA samples on the cap of the bottle. The results of the PolyHEMA experiment can be seen in Table 8. The graphical view for Table 8 can be seen in Figure 4.9 since it makes the visualization of the values in the table, much easier. Figure 4.10 shows the graph with the analysis of the data for the two-trial experiment.

It can be observed that there is fluctuation in the phase and voltage levels observed. This can be related to the fact that biofilm growth on the side of the plastic box is not consistent and they occasionally fall off from the side walls. As the biofilm build up grows on the side of the walls, the ultrasound sensor voltage and phase shift decrease since sound experiences higher attenuation when passing between medium with different refracting indices. Each time ultrasonic waves approaches a medium with high refractive index, only a small portion of the wave passes through the substance and the rest is reflected [84]. However, this small magnitude is enough to interpret the presence of a foreign element in a testing medium. This trend is also observed when the experiment is repeated, and this analysis can be seen in Figure 4.8. The PolyHEMA experiment did not have good correlation relationship because the thickness of the solidified PolyHEMA differed between each trial. While the voltage and phase decreased with the increase in thickness, the two trials did not have a good correlation between each other. The correlation between the trials for the voltage and phase data (from the function generator) indicated a weak negative linear relationship with the coefficient values of -0.26 and -0.37 respectively. On the other hand, the relation between the trials for the voltage and phase (from the TDC board) indicated a weak to

moderate relationship with coefficient values 0.10 and 0.46 respectively. There exists no interrelationship between the data since the PolyHEMA solidified differently (i.e. different thickness) for each trial.

Table 9: Results of the PolyHEMA experiment. The sensor data was recorded consecutively for PolyHEMA buildup of different thickness. The data comprises of change in Phase shift and Voltage change.

Thickness of PolyHEMA (mm)	Function Generator Phase Shift Change (ns)	Function Generator Change in Voltage (V)	TDC Phase Shift Change (ns)	TDC Change in Voltage (V)
0.114	-0.028	-0.36	2.533	1.04
0.190	-0.074	-0.16	-0.216	0.00
0.347	0.176	0.04	-1.066	-0.68
0.411	-0.190	0.00	-0.245	0.00
0.468	-0.606	-1.25	-0.501	-0.61
0.515	0.060	0.68	2.037	0.92
0.605	-0.122	-1.53	0.284	0.20
0.664	-0.052	0.32	1.108	0.44
0.684	-0.780	-0.57	1.263	0.56
0.822	-0.221	-1.20	-0.068	0.08

a.

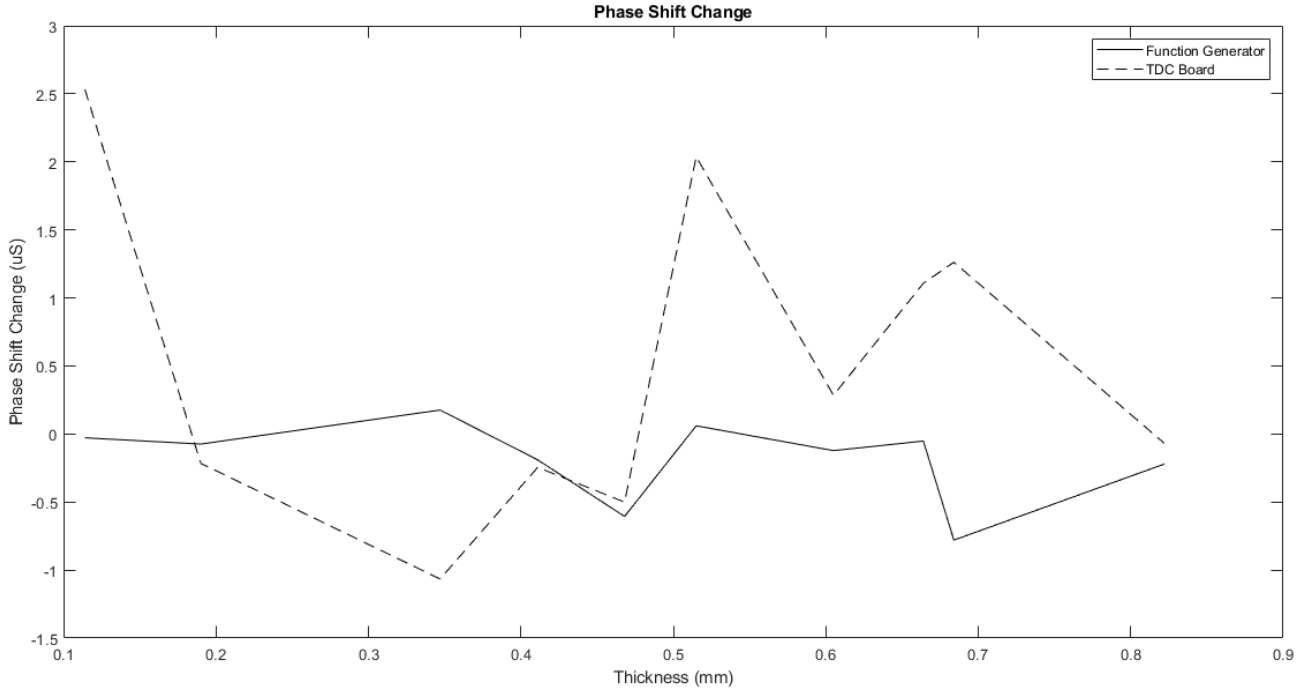

b.

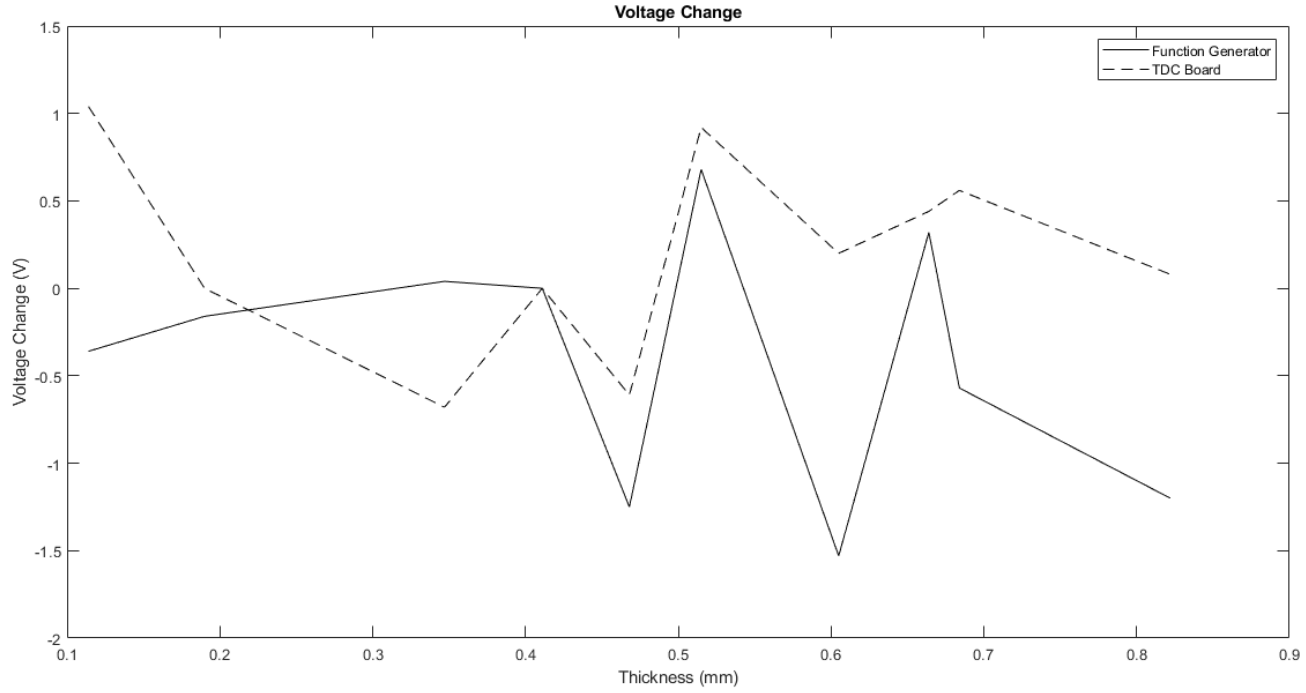

Figure 4.9: (a) Graph showing the variations in the phase change in increasing order of thickness (mm) of PolyHEMA. The phase variations are in the micro-second range. (b) Graph showing the variations in the voltage change in increasing orders of thickness (mm). The bold line represents the measurements when the sensors are powered by the Function generator whereas the dashed line are those when the sensors are powered by the TDC evaluation board.

a.

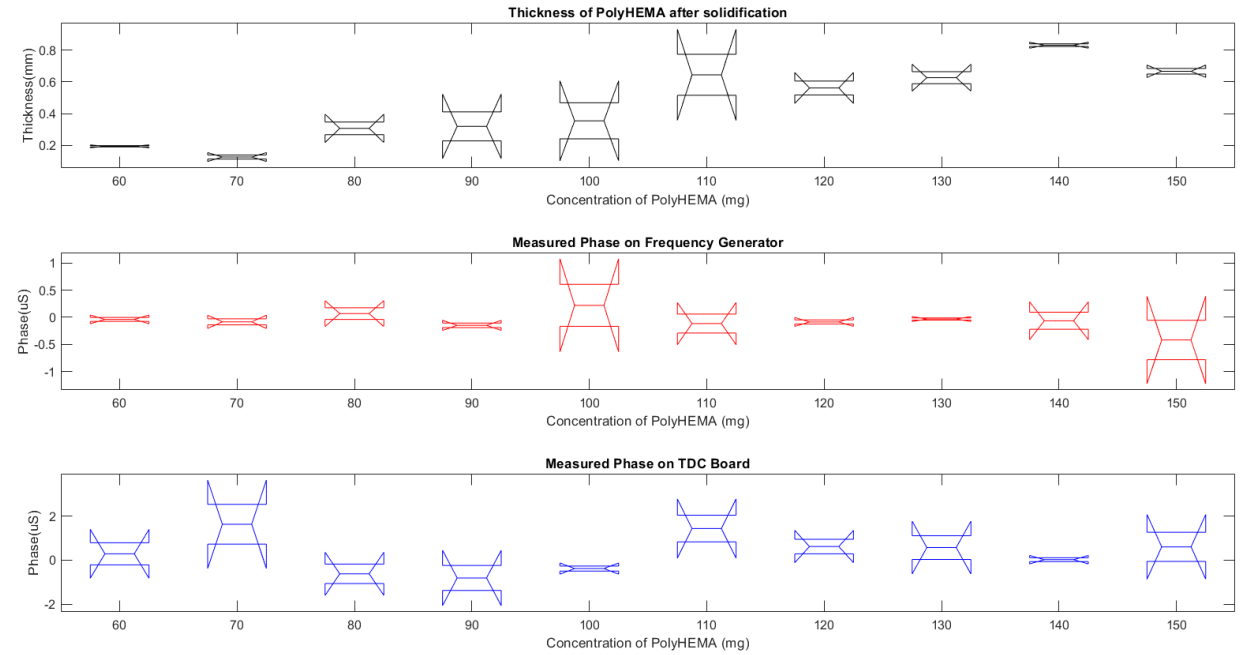

b.

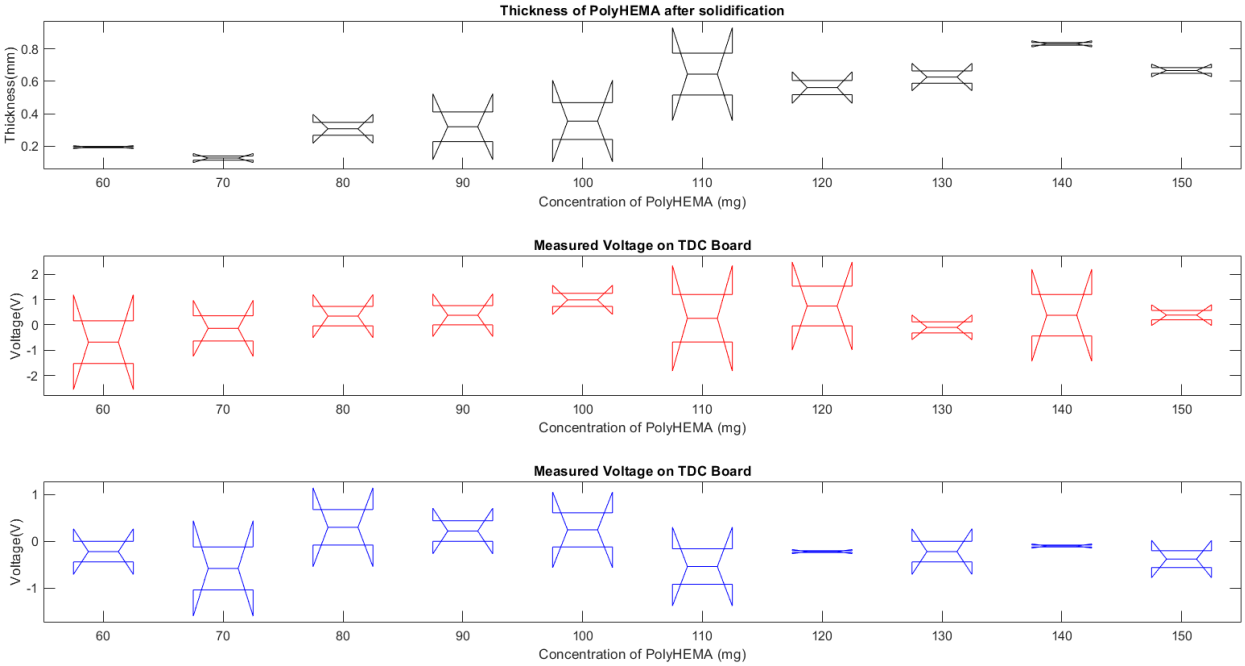

Figure 4.10: (a) Graph showing the analysis of variations in the phase change in increasing order of thickness (mm) of PolyHEMA when the trails was repeated twice. The phase variations are in the micro-second range. (b) Graph showing the variations in the voltage change in increasing orders of thickness (mm) when the experiment was repeated twice.

4.3 Results of the solubility test experiment

The solubility experiment consists of a small plastic chamber as shown in Figure 4.11 with DI water. Specific amount of salt is added to this solution step by step and the variations in the parameters were noted. The quantity of the salt was dissolved in the DI water consecutively in small measures. The readings can be seen recorded in Table 9.

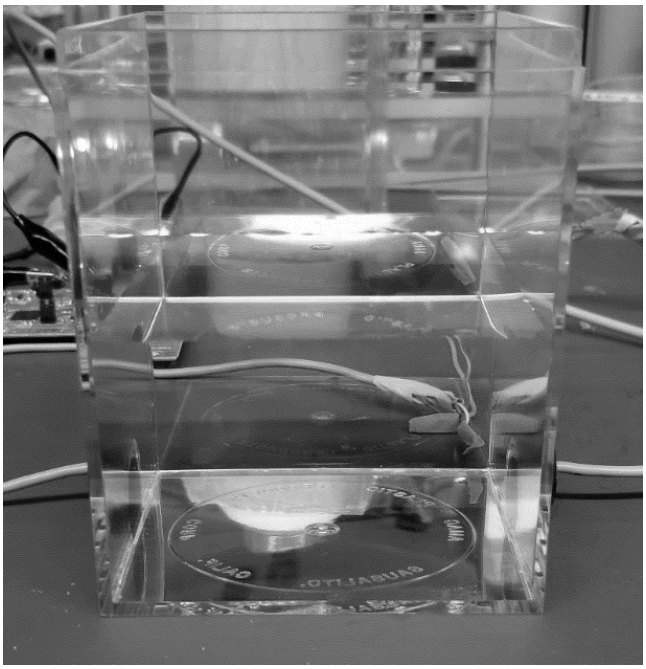

Figure 4.11: Solubility experiment setup. Plastic chamber with ultrasound sensors on either side.

From the table below, it is evident that the phase shift is the best method to observe the effect of solubility on sensor data. The phase shift for both the function generator and the TDC board can be used to interpret the effect of solubility. As the number of salt increases in the solution, the phase shift observed decreases. The output voltage, however, is not a good indicator of the solubility. The change in phase shift is evident with the increase in salinity (or amount of dissolved salt in water). As the amount of dissolved salt in water increases, the presence of solid

particles increases thus having a higher attenuation causing the phase shift to decrease since attenuation of signal amplitude and intensity is reduced by the spreading of the wave and differences in medium when sound travels between mediums [18]. In this case the sound waves travel from a liquid into a solid particle (salt) and then back to liquid. The fluctuations in voltage can be related to the placement of the sensors. It is possible that when the sonic wave passed through the medium, it passed different amounts of suspended particles on a given test when compared to previous test. The same trend can be observed when the experiment was repeated multiple times. The graphical analysis using the boxplot analysis with the notch filter on can be seen in Figure 4.12.

Table 10: Results of the solubility experiment. The sensor data was recorded when a specific weight of salt was added in small measures. The data comprises of change in Phase shift and Voltage change.

Amount of Salt in Water (g)	Function Generator Phase Shift (μs)	Function Generator Voltage (V)	TDC Phase Shift (μs)	TDC Voltage (V)
0	60.258	9.15	119.043	2.35
1	60.152	9.05	118.906	2.45
2	60.078	9.15	118.733	2.45
3	59.951	9.00	118.567	2.50
4	59.883	8.85	118.392	2.50
5	59.794	9.05	118.211	2.45

The Pearson-correlation data for the solubility experiment for multiple trials are recorded in Table 11. There is a strong relationship between the data (phase and TDC phase) which indicates that the phase measured from both the function generator and the TDC board can be used to detect the increase in the amount of dissolved or suspended particles in water. The voltage data measured from both the function generator and the TDC board can be used to detect the changes, but the relationship between the data is not as strong as the phase data.

Table 11: Pearson-correlation data for the solubility experiment. A strong relationship exists when the Pearson correlation index is between 0.7 and 1. '*' indicates moderate or weak relationship or correlation of data between trials. '**' indicates a weak negative correlation where the trial data behaves in opposite direction.

	Trial 1	Trial 2	Trial 3
Voltage (V)	1.00	0.63*	-0.28**
TDC Voltage (V)	1.00	0.63*	0.59*
Phase (μs)	1.00	1.00	1.00
TDC Phase (μs)	1.00	1.00	1.00

a.

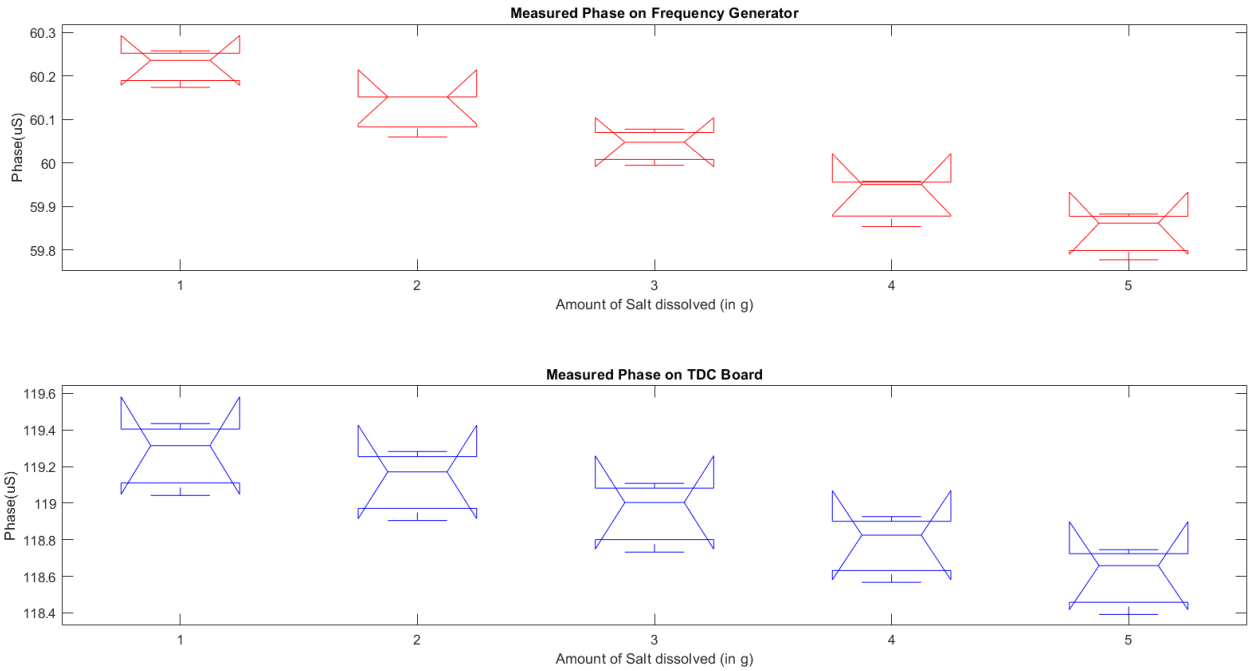

b.

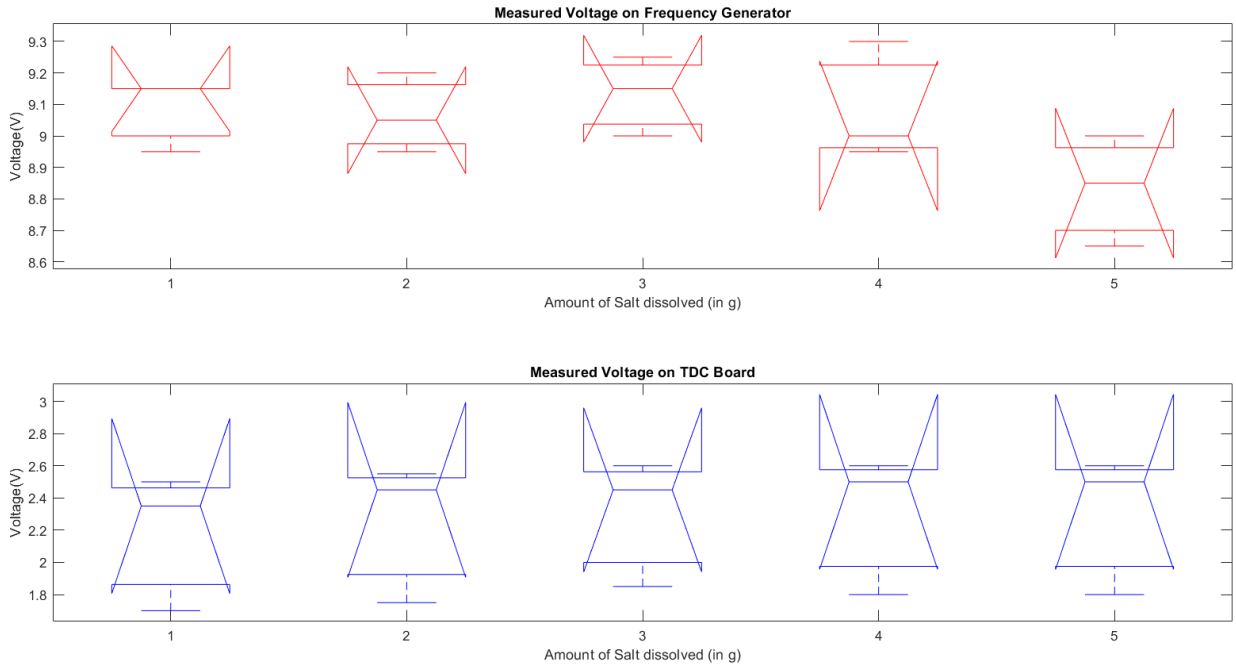

Figure 4.12: (a) Graph showing the variations in the Phase change when the amount (g) of dissolved salt in water. The phase variations are in the micro-second range. (b) Graph showing the variations in the Voltage change when the amount (g) of dissolved salt increases. The red trace represents the measurements when the sensors are powered by the Function generator whereas the blue trace represents those when the sensors are powered by the TDC evaluation board.

4.4 Results of the experiments to determine the effect of different materials on sensor data

The change in materials experiment comprises of a pipe design involving three different materials: PVC, Copper and Galvanized Iron. The pipe design is filled with water and the sensors are placed on either side of the pipe.

For the 2” piping system, PVC was taken as the control and the change in sensor data was recorded to identify the attenuation in these objects. Figure 3.8 shows the experiment setup involving piping structures of all three materials.

The results of the experiment with 2” piping design are recorded in Table 10. It is evident that Galvanized Iron has the highest attenuation on the ultrasound signal. PVC has the least attenuation effect among the three materials. It can also be noted that there is a distinguishable phase shift when the type of material is changed.

Table 12: Results of the change in materials, single trial experiment. The piping design used had a thickness of 2” and data was recorded using the function generator and oscilloscope

Type of Material	Phase Shift (μs)	Output Voltage (mV)
PVC	40.636	840
Copper	37.440	105
Galvanized Iron	29.240	70

For the 3” piping system, PVC was taken as the control and the change in sensor data was recorded to identify the attenuation in these objects. Figure 3.9 shows the experiment setup involving piping structures of the two materials.

The results of the experiment with 3" piping design are recorded in Table 11. It is evident that Galvanized Iron has the highest attenuation on the ultrasound signal and has a significant change in the phase shift.

Table 13: Results of the change in materials, single trial experiment. The piping design used had a thickness of 3" and data was recorded using the function generator and oscilloscope.

Type of Material	Phase Shift (μs)	Output Voltage (mV)
PVC	61.660	580
Galvanized Iron	20.060	130

The results clearly suggest that some materials have more attenuation effects on the ultrasound wave compared to the other and the size of the wall thickness of these materials also impact the sensor output. This relates to the fact that sound travels through materials under the influence of sound pressure and the molecules and atoms of different substances are bound elastically to one another differently. Some sound pressure is required to overcome this bond and the excess pressure causes the wave propagation through the solid [85]. In our case, the PVC has less bonding at the atomic level while that of Iron is significantly higher or the acoustic impedance of Iron is significantly higher than that of PVC. Copper has an acoustic impedance that is greater than that of PVC and slightly lower than Iron. The acoustic impedance data is available from the UT Material Properties charts of different materials available in the NDT resource center [86]. The acoustic impedance of

Iron = $45.43 \times 10^5 \frac{g}{cm^2-sec}$

Copper = $45.43 \times 10^5 \frac{g}{cm^2-sec}$

Polystyrene (or PVC) = $2.937 \times 10^5 \frac{g}{cm^2-sec}$

From all the experiment results described above, the biofilm experiment and the solubility experiment showed good interrelationship between trials and the trend was observed to be repeated for each trial. It was observed that the results from the function generator were more reliable than the results observed from the TDC board. This could be related to the fact that the TDC board is limited to trigger the ultrasound sensor with a maximum voltage of 5 V while the function generator can be used to trigger the ultrasound sensor with a much higher voltage. The output reading of the receiver sensors can be observed on the oscilloscope screen as soon as the transmitter sensors are triggered. In other words, it takes less than a second to observe the output.

Chapter 5

Conclusions

The experimental results described above support the hypothesis that the design involving the two ultrasound sensors placed on either side of a piping system can be used for the detection of thin biofilm. It is evident that there are certain ultrasound sensors that are not compatible with the design developed in the laboratory i.e. the HC-SR04 Arduino sensors cannot be used for the detection of biofilm in test chambers with water as a medium. In this phase, ultrasound sensors with frequencies of 1 MHz were tested with the help of small plastic chambers developed in the laboratory and multiple tests helped conclude the reliability of the design of the system. It was observed that as the material of the pipe changes, the sensor output changes accordingly. This implied that the sensor data must be treated differently according to the material of the pipe on which measurements are recorded. From all the experiments, the voltage and phase data observed from the function generator can be used as an indicator of the presence of biofilm in closed piping systems due to strong interrelationship between observed between the data observed from both the function generator and the TDC board. This indicates that the sensor arrangement can detect a change in the initial state of the system by the observation of two parameters voltage and phase. For example, when the closed system has no biofilm formation, the measured voltage and phase are recorded as the initial value and this value changes relative to the thickness of the biofilm formation inside the closed piping system. At present, the sensor arrangement can detect thickness greater than 40 μm (which can be related to Stage 2 or Stage 3 of biofilm growth). This data is obtained in real-time (or less than a second, i.e. The output of the receiver sensors can be observed

on the oscilloscope as soon as the transmitter sensor is triggered) The sensitivity of the sensors can be improved by triggering the ultrasound sensors with a higher voltage and using digital signal processing techniques.

In the next phase (Phase 2) of the research, a filter window (a digital signal processing technique) will be used to focus the ultrasound signal onto the surface of the pipe to reduce the effect of attenuation as much as possible. Further tests will be conducted exclusively for the detection of the presence of biofilms on the simulated piping developed inside the laboratory. At the end of Phase-II of the project, a prototype will be built that can be used in a real-world scenario for the measurement of biofilm build-up. This prototype will be designed such that the sensors are triggered remotely, and the output of the data can be measured from a smart device for users to take corrective actions.

References

[1] J. W. Costerton, G. G. Geesey and K. J. Cheng, "How bacteria stick," *Scientific American,* vol. 238, pp. 86-96, 1978.

[2] J. W. Costerton and H. M. Lappin-Scott, "Introduction to microbial biofilms," in *Microbial biofilms*, Cambridge, Cambridge University Press, 1995, pp. 1-11.

[3] J. W. Costerton, K. J. Cheng, G. G. Geesey, T. I. Ladd, J. C. Nickel, M. Dasgupta and T. J. Marrie, "Bacterial biofilms in nature and disease," *Annual Reviews in Microbiology,* vol. 41, pp. 435-464, 1987.

[4] K. C. Marshall and W. G. Characklis, Wiley Series in Ecological and Applied Microbiology, New York: John Wiley & Sons Ltd., 1990.

[5] J. W. Costerton, P. S. Stewart and E. P. Greenberg, "Bacterial Biofilms: A Common Cause of Persistent Infections," *Science Magazine,* vol. 284, no. 5418, pp. 1318-1322, 1999.

[6] L. Hall-Stoodley, J. W. Costerton and P. Stoodley, "Bacterial biofilms: from the Natural environment to infectious diseases," *Nature Reviews Microbiology,* vol. 2, pp. 95-108, 2004.

[7] S. Marchand, J. De Block, V. De Jonghe, A. Coorevits, M. Heyndrickx and L. Herman, "Biofilm Formation in Milk Production and Processing Environments; Influence on Milk Quality and Safety," *Comprehensive Reviews in Food Science and Food Safety,* vol. 11, no. 2, pp. 133-147, 2012.

[8] R. Murga, P. S. Stewart and D. Daly, "Quantitative analysis of biofilm thickness variability," *Biotechnology and Bioengineering,* vol. 45, no. 6, pp. 503-510, 1995.

[9] P. S. Stewart, "Theoretical aspects of antibiotic diffusion into microbial biofilms," *Antimicrobial Agents and Chemotherapy,* vol. 40, no. 11, pp. 2517-2522, 1996.

[10] J. C. Nickel, I. Ruseska, J. B. Wright and J. W. Costerton, "Tobramycin resistance of Pseudomonas aeruginosa cells growing as a biofilm on urinary catheter material," *Antimicrobial Agents and Chemotherapy,* vol. 27, no. 4, pp. 619-624, 1985.

[11] T. J. Marrie and J. W. Costerton, "A scanning and transmission electron microscopic study of the surfaces of intrauterine contraceptive devices," *American Journal of Obstetrics and Gynecology,* vol. 146, no. 4, pp. 384-394, 1983.

[12] "Biofilms: Survival Mechanisms of Clinically Relevant Microorganisms," *Clinical Microbiology Reviews*, vol. 15, no. 2, pp. 167-193, 2002.

[13] I. Williams, W. A. Venables, D. Lloyd, F. Paul and I. Critchley, "The effects of adherence to silicone surfaces on antibiotic susceptibility in Staphylococcus aureus," *Microbiology,* vol. 143, pp. 2407-2413, 1997.

[14] H. Ceri, M. E. Olson, C. Stremick, R. R. Read, D. Morck and A. Buret, "The Calgary Biofilm Device: New Technology for Rapid Determination of Antibiotic Susceptibilities of Bacterial Biofilms," *Journal of Clinical Microbiology,* vol. 37, no. 6, pp. 1771-1776, 1999.

[15] M. Vorachit, K. Lam, P. Jayanetra and J. W. Costerton, "Resistance of Pseudomonas pseudomallei growing as a biofilm on silastic discs to ceftazidime and co-trimoxazole," *Antimicrobial Agents and Chemotherapy,* vol. 37, no. 9, pp. 2000-2002, 1993.

[16] T. Larsen and N.-E. Fiehn, "Resistance of Streptococcus sanguis biofilms to antimicrobial agents," *APMIS,* vol. 104, pp. 280-284, 1996.

[17] S. M. Bartsch, L. Asti, S. Nyathi, M. L. Spiker and B. Y. Lee, "Estimated Cost to a Restaurant of a Foodborne Illness Outbreak," John Hopkins Bloomberg School of Public Health, 16 April 2018. [Online]. Available: https://www.jhsph.edu/news/news-releases/2018/a-foodborne-illness-outbreak-could-cost-a-restaurant-millions-study-suggests.html. [Accessed 5 November 2018].

[18] "Waterborne Diseases Could Cost over $500 Million Annually in U.S.," Centers for Disease Control and Prevention, 14 July 2010. [Online]. Available: https://www.cdc.gov/media/pressrel/2010/r100714.htm. [Accessed 5 November 2018].

[19] J. Sheng, E. Malkiel and J. Katz, "Digital holographic microscope for measuring three-dimensional particle distributions and motions," *Applied Optics,* vol. 45, no. 16, pp. 3893-3901, 2006.

[20] H. C. Berg and D. A. Brown, "Chemotaxis in Escherichia coli analysed by three-dimensional tracking," *Nature,* vol. 239, no. 5374, pp. 500-504, 1972.

[21] M. Molaei, M. Barry, R. Stocker and J. Sheng, "Failed escape: Solid surfaces prevent tumbling of Escherichia coli,," *Physical Review Letters,* vol. 113, no. 6, pp. 068103 1-6, 2014.

[22] K. M. Taute, S. Gude, S. J. Tans and T. S. Shimizu, "High-throughput 3D tracking of bacteria on a standard phase contrast microscope," *Nature Communications,* vol. 6, p. 8776, 2015.

[23] L. Turner, L. Ping, M. Neubauer and H. C. Berg, "Visualizing Flagella while Tracking Bacteria," *Biophysical Journal,* vol. 111, no. 3, pp. 630-639, 2016.

[24] S. Schlafer and R. L. Meyer, "Confocal microscopy imaging of the biofilm matrix," *Journal of Microbiological Methods,* vol. 138, pp. 50-59, 2017.

[25] R. Zuriani, S. Vigneswari, M. N. M. Azizan, M. I. A. Majid and A. A. Amirul, "A high throughput Nile red fluorescence method for rapid quantification of intracellular bacterial polyhydroxyalkanoates," *Biotechnology and Bioprocess Engineering,* vol. 18, no. 3, pp. 472-478, 2013.

[26] N. Kamjunke, U. Spohn, M. Futing, G. Wagner, E.-M. Scharf, S. Sandrock and B. Zippel, "Use of confocal laser scanning microscopy for biofilm investigation on paints under field conditions," *International Biodeterioration and Biodegradation,* vol. 69, pp. 17-22, 2012.

[27] J. R. Lawrence, T. R. Neu and G. D. W. Swerhone, "Application of multiple parameter imaging for the quantification of algal, bacterial and exopolymer components of microbial biofilms," *Journal of Microbiological Methods,* vol. 32, no. 3, pp. 253-261, 1998.

[28] J. Xiao and H. Koo, "Structural organization and dynamics of exopolysaccharide matrix and microcolonies formation by Streptococcus mutans in biofilms," *Journal of Applied Microbiology,* vol. 108, no. 6, pp. 2103-2113, 2010.

[29] W. Hu, L. Li, S. Sharma, J. Wang, I. McHardy, R. Lux, Z. Yang, X. He, J. K. Gimzewski, Y. Li and W. Shi, "DNA Builds and Strengthens the Extracellular Matrix in Myxococcus xanthus Biofilms by Interacting with Exopolysaccharides," *PLoS ONE,* vol. 7, no. 12, p. 51905, 2012.

[30] G. Hidalgo, A. Burns, E. Herz, A. G. Hay, P. L. Houston, U. Wiesner and L. W. Lion, "Functional tomographic fluorescence imaging of pH microenvironments in microbial biofilms by use of silica nanoparticle sensors," *Applied Environmental Microbiology,* vol. 75, no. 23, pp. 7426-7435, 2009.

[31] M. A. Acosta, M. Velasquez, K. Williams, J. M. Ross and J. B. Leach, "Fluorescent silica particles for monitoring oxygen levels in three-dimensional heterogeneous cellular structures," *Biotechnology and Bioengineering*, vol. 109, no. 10, pp. 2663-2670, 2012.

[32] J. M. Vroom, K. J. De Grauw, H. C. Gerritsen, D. J. Bradshaw, P. D. Marsh, G. K. Watson, J. J. Birmingham and C. Allison, "Depth penetration and detection of pH gradients in biofilms by two-photon excitation microscopy," *Applied Environmental Microbiology*, vol. 65, no. 8, pp. 3502-3511, 1999.

[33] J. Xiao, M. I. Klein, M. L. Falsetta, B. Lu, C. M. Delahunty, J. R. Yates III, A. Heydom and H. Koo, "The Exopolysaccharide Matrix Modulates the Interaction between 3D Architecture and Virulence of a Mixed-Species Oral Biofilm," *PLoS Pathogens*, vol. 8, no. 4, 2012.

[34] S. Takenaka, B. Pitts, H. M. Trivedi and P. S. Stewart, "Diffusion of macromolecules in model oral biofilms," *Applied Environmental Microbiology*, vol. 75, no. 6, pp. 1750-1753, 2009.

[35] P. Stoodley, D. de Beer and Z. Lewandowski, "Liquid flow in biofilm systems," *Applied Environmental Microbiology*, vol. 60, no. 8, pp. 2711-2716, 1994.

[36] A. Birjiniuk, N. Billings, E. Nance, J. Hanes, K. Ribbeck and P. S. Doyle, "Single particle tracking reveals spatial and dynamic organization of the Escherichia coli biofilm matrix," *New Journal of Physics*, vol. 16, no. 8, 2014.

[37] F. Waharte, K. Steenkeste, R. Briandet and M. P. Fontaine-Aupart, "Diffusion measurements inside biofilms by image-based fluorescence recovery after photobleaching (FRAP) analysis with a commercial confocal laser scanning microscope," *Applied Environmental Microbiology*, vol. 76, no. 17, pp. 5860-5869, 2010.

[38] S. Daddi Oubekka, R. Briandet, M. P. Fontaine-Aupart and K. Steenkeste, "Correlative Time-Resolved Fluorescence Microscopy To Assess Antibiotic Diffusion-Reaction in Biofilms," *Antimicrobial Agents and Chemotherapy*, vol. 56, no. 6, pp. 3349-3358, 2012.

[39] R. Briandet, P. Lacroix-Gueu, M. Renault, S. Lecart, T. Meylheuc, E. Bidnenko, K. Steenkeste, M. N. Bellon-Fontaine and M. P. Fontaine-Aupart, "Fluorescence correlation spectroscopy to study diffusion and reaction of bacteriophages inside biofilms," *Applied Environmental Microbiology*, vol. 74, no. 7, pp. 2135-2143, 2008.

[40] M. Fletcher, "The effects of culture concentration and age, time, and temperature on bacterial attachment to polystyrene," *Canadian Journal of Microbiology*, vol. 23, no. 1, pp. 1-6, 2011.

[41] D. Djordjevic, M. Wiedmann and L. A. Mclandsborough, "Microtiter Plate Assay for Assessment of Listeria monocytogenes Biofilm Formation," *Applied and Environmental Microbiology*, vol. 68, no. 6, pp. 2950-2958, 2002.

[42] H. Ceri, M. E. Olson, C. Stremick, R. R. Read, D. Morck and A. Buret, "The Calgary Biofilm Device: New Technology for Rapid Determination of Antibiotic Susceptibilities of Bacterial Biofilms," *Journal of Clinical Microbiology*, vol. 37, no. 6, pp. 1771-1776, 1999.

[43] P. Chavant, B. Gaillard-Martinie, R. Talon, M. Hebraud and T. Bernardi, "A new device for rapid evaluation of biofilm formation potential," *Journal of Microbiological Methods*, vol. 68, no. 3, pp. 605-612, 2007.

[44] J. P. Salanitro and J. S. Hokanson, "Tubular biofilm reactor". Houston, TX Patent H000831, 02 October 1990.

[45] W. F. McCoy and J. D. Bryers, "Observations of fouling biofilm formation," *Canadian Journal of Microbiology,* vol. 27, no. 9, pp. 910-917, 1981.

[46] M. Wagnera, N. P. Ivlevab, C. Haischb, R. Niessnerb and H. Horn, "Combined use of confocal laser scanning microscopy (CLSM) and Raman microscopy (RM): Investigations on EPS – Matrix," *Water Research,* vol. 43, pp. 63-76, 2009.

[47] S. Ramya, R. P. George, R. V. Subba Rao and R. K. Dayal, "Detection of algae and bacterial biofilms formed on titanium surfaces using micro-Raman analysis," *Applied Surface Science,* vol. 256, pp. 5108-5115, 2010.

[48] F. Shiraishi, B. Zippel, T. R. Neu and G. Arp, "In situ detection of bacteria in calcified biofilms using FISH and CARD-FISH," *Journal of Microbiological Methods,* vol. 75, pp. 103-108, 2008.

[49] C. T. Nguyen, S. R. Robinson, W. Jung, M. A. Novak, S. A. Boppart and J. B. Allen, "Investigation of bacterial biofilm in the human middle ear using optical coherence tomography and acoustic measurements," *Hearing Research,* vol. 301, pp. 193-200, 2013.

[50] H. Shemesh, D. E. Goertz, L. W. M. van der Sluis, N. de Jong, M. K. Wu and P. R. Wesselink, "High frequency ultrasound imaging of a single-species biofilm," *Journal of Dentistry,* vol. 35, pp. 673-678, 2007.

[51] J. Azeredo, N. F. Azevedo, R. Briandet, N. Cerca, T. Coenye, A. R. Costa, M. Desvaux, G. Di Bonaventura, M. Hebraud, Z. Jaglic, M. Kacaniova, S. Knochel, A. Lourenco, F. Mergulhao, R. L. Meyer, G. Nychas, M. Simoes, O. Tresse and C. Sternberg, "Critical review on biofilm methods," *Critical Reviews in Microbiology,* vol. 43, no. 3, pp. 313-351, 2017.

[52] "PDMS Polymers," Sigma-Aldrich, [Online]. Available: https://www.sigmaaldrich.com/materials-science/material-science-products.html?TablePage=113790985. [Accessed 12 June 2018].

[53] "Polydimethyl siloxane," Dimethicone, [Online]. Available: https://www.dimethicone.net/polydimethylsiloxane/. [Accessed 15 June 2018].

[54] A. Augustyn, P. Bauer, B. Duignan, A. Eldridge, E. Gregersen, J. E. Luebering, A. McKenna, M. Petruzzello, J. P. Rafferty, M. Ray, K. Rogers, A. Tikkanen, J. Wallenfeldt, A. Zeidan and A. Zelazko, "Encyclopaedia Britannica," Encyclopaedia Britannica Inc., 24 October 2012. [Online]. Available: https://www.britannica.com/science/polyHEMA. [Accessed 16 October 2018].

[55] M. R. Islam, L. G. Bach, J. M. Park, S.-S. Hong and K. T. Lim, "Synthesis and characterization of poly(HEMA-co-MMA)-g-POSS nanocomposites by combination of reversible addition fragmentation chain transfer polymerization and click chemistry," *Journal of Applied Polymer Science,* vol. 127, no. 3, pp. 1569-1577, 2013.

[56] M. T. W., T. B. J., L. M. J. and R. D. A., "Requirements for cell spreading on polyHEMA coated culture substrates," *Cell Biology International Reports,* vol. 8, no. 2, pp. 151-159, 1984.

[57] P. D. -I. V. Deutsch, "History of NDT-Instrumentation," AIPnD, 2000. [Online]. Available: https://www.ndt.net/article/wcndt00/papers/idn378/idn378.htm. [Accessed 15 October 2018].

[58] D. M. A. Morgan, "Ultrasound (Introduction)," Radiopaedia, [Online]. Available: https://radiopaedia.org/articles/ultrasound-introduction?lang=us. [Accessed October 26 2018].

[59] A. Aubry and A. Derode, "Multiple Scattering of Ultrasound in Weakly Inhomogeneous Media: Application to Human Soft Tissues," *arXiv.org 129.1,* pp. 225-233, 2011.

[60] M. Pakula, "Attenuation and dispersion of ultrasound in cancellous bone. Theory and experiment," *Journal of the Acoustical Society of America,* vol. 140, no. 4, p. 3080, 2016.

[61] M. Dzida, E. Zorebksi, M. Zorebski, M. Zarska, M. Geppert-Rybczynska, M. Chorazewski, J. Jacquemin and I. Cibulka, "Speed of Sound and Ultrasound Absorption in Ionic Liquids," *Chemical Reviews,* vol. 117, pp. 3883-3929, 2017.

[62] "Basic Principles of Ultrasonic Testing," NDT Resource Center, 1996. [Online]. Available: https://www.nde-ed.org/EducationResources/CommunityCollege/Ultrasonics/Introduction/description.htm. [Accessed 2 February 2018].

[63] "Wave Propagation," NDT Resource Center, 1996. [Online]. Available: https://www.nde-ed.org/EducationResources/CommunityCollege/Ultrasonics/Physics/wavepropagation.htm. [Accessed 25 August 2018].

[64] D. Y. Weerakkody and D. J. Cheng, "Reflection," Radiopaedia, [Online]. Available: https://radiopaedia.org/articles/reflection?lang=us. [Accessed 28 August 2018].

[65] D. H. Knipe and D. P. O'Gorman, "Refraction," Radiopaedia, [Online]. Available: https://radiopaedia.org/articles/refraction?lang=us. [Accessed 29 August 2018].

[66] "Rail Inspection," NDT Resource Center, 1996. [Online]. Available: https://www.nde-ed.org/EducationResources/CommunityCollege/Ultrasonics/SelectedApps/railinspection.htm. [Accessed 5 February 2018].

[67] S. T. V. Sim, S. R. Suwarno, Y. X. S. Lim, W. X. J. Lim, T. H. Chong and A. G. Fane, "Development of Novel Acoustic Sensor for Early Detection of Biofouling in Reverseosmosis Systems," *Procedia Engineering,* vol. 44, pp. 562-566, 2012.

[68] J. Li, D. K. Hallbauer and R. D. Sanderson, "Direct Monitoring of membrane fouling and cleaning during ultrafiltration using a Non-invasive Ultrasonic Technique," *Journal of Membrane Science,* vol. 215, pp. 33-52, 2003.

[69] E. Kunjundzic, C. A. Fonseca, E. A. Evans, M. Peterson, A. R. Greenberg and M. Hernandez, "Ultrasonic monitoring of early-stage biofilm growth on polymeric surfaces," *Journal of Microbiological Methods,* vol. 68, pp. 458-467, 2007.

[70] S. T. Sim, S. R. Suwarno, Y. X. Lim, T. H. Chong and A. G. Fane, "Development of novel acoustic sensor for early detection of biofouling in reverse-osmosis systems," *Procedia Engineering,* vol. 44, pp. 562-566, 2012.

[71] H. Shemesh, D. E. Goertz, L. W. van der Sluis, N. de Jong, M. K. Wu and P. R. Wesselink, "High frequency ultrasound imaging of a single-species biofilm," *Journal of Dentistry,* vol. 35, pp. 673-678, 2007.

[72] F. (. D. Seida, C. (. D. Flocken, P. (. D. Bierganns and M. (. D. D. Schultz, "Device and Method for detecting Deposits". United States Patent 20150000407, 1 January 2015.

[73] P. (. D. Bierganns and M. M. (. a. d. R. D. Broecher, "Device and Method for detecting and analyzing Deposits". United States Patent 20160076990, 17 March 2016.

[74] "1ME21TR-1," Osenon, [Online]. Available: https://www.osenon-ultrasonicsensors.com/a1me21tr-1s. [Accessed 10 July 2018].

[75] Cytron Technologies Sdn. Bhd., "Product User's Manual - HCSR04 Ultrasonic sensor," May 2013. [Online]. Available: https://docs.google.com/document/d/1Y-yZnNhMYy7rwhAgyL_pfa39RsB-x2qR4vP8saG73rE/edit. [Accessed 6 June 2018].

[76] "Ultrasonic Sensing Water Flow/Level/Concentration Evaluation Module," Texas Instruments, 2015. [Online]. Available: http://www.ti.com/tool/TDC1000-TDC7200EVM. [Accessed 03 March 2018].

[77] "TDC 1000," Texas Instruments, 2015. [Online]. Available: http://www.ti.com/product/TDC1000/description. [Accessed 03 March 2018].

[78] V. Viswanathan, "Interleaved Short Time Measurements Using TDC7200," Texas Intruments, January 2016. [Online]. Available: http://www.ti.com/lit/an/snaa288/snaa288.pdf. [Accessed 19 August 2018].

[79] Texas Instruments, "TDC7200 Time-to-Digital Converter for Time-of-Flight Applications in LIDAR, Magnetostrictive and Flow Meters," March 2016. [Online]. Available: http://www.ti.com/lit/ds/symlink/tdc7200.pdf. [Accessed 20 August 2018].

[80] "Arduino Uno Rev3," Arduino, [Online]. Available: https://store.arduino.cc/usa/arduino-uno-rev3/. [Accessed 01 June 2018].

[81] "AFG-2225 Dual-Channel Arbitrary Function Generator," GwINSTEK, [Online]. Available: https://www.gwinstek.com/en-US/products/detail/AFG-2225. [Accessed 01 August 2018].

[82] "MSOX2024A Mixed Signal Oscilloscope: 200 MHz, 4 Analog Plus 8 Digital Channels," Keysight Technologies, [Online]. Available: https://www.keysight.com/en/pdx-x201838-pn-MSOX2024A/mixed-signal-oscilloscope-200-mhz-4-analog-plus-8-digital-channels?pm=spc&nid=-32542.1150191&cc=US&lc=eng. [Accessed 01 August 2018].

[83] United States Environmental Protection Agency, "Method 1603: Escherichia coli (E. coli) in Water by Membrane Filtration Using Modified membrane-Thermotolerant Escherichia coli Agar (Modified mTEC," September 2014. [Online]. Available: https://www.epa.gov/sites/production/files/2015-08/documents/method_1603_2009.pdf. [Accessed 02 May 2018].

[84] "Refraction and Snell's Law," NDT Resource Center, 1996. [Online]. Available: https://www.nde-ed.org/EducationResources/CommunityCollege/Ultrasonics/Physics/refractionsnells.htm. [Accessed 6 February 2018].

[85] "Acoustic Impedance," NDT Resource Center, 1996. [Online]. Available: https://www.nde-ed.org/EducationResources/CommunityCollege/Ultrasonics/Physics/acousticimpedance.htm. [Accessed 9 February 2018].

[86] "UT Material Properties," NDT Resource Center, 1996. [Online]. Available: https://www.nde-ed.org/EducationResources/CommunityCollege/Ultrasonics/Reference%20Information/matproperties.htm. [Accessed 12 February 2018].

[87] Y. H. An and R. J. Friedman, "Laboratory methods for studies of bacterial adhesion," *Journal of Microbiological Methods*, vol. 30, no. 2, pp. 141-152, 1997.

[88] J. W. Costerton, Z. Lewandowski, D. E. Caldwell, D. R. Korber and H. M. Lappin-Scott, "Microbial Biofilms," *Annual Review of Microbiology*, vol. 49, pp. 711-745, 1995.

[89] T. Lewis, "5 Fascinating Facts About Fetal Ultrasounds," Live Science, 16 May 2013. [Online]. Available: https://www.livescience.com/32071-history-of-fetal-ultrasound.html. [Accessed 12 August 2018].

[90] "A quick history of Ultrasounds," Two Views, [Online]. Available: https://two-views.com/ultrasounds/history.html. [Accessed 25 August 2018].

[91] M. Strathmann, T. Griebe and H.-C. Flemming, "Artificial biofilm model – A useful tool for biofilm research," Applied Microbiology and Biotechnology, vol. 54, no. 2, pp. 231-7, 2000.

[92] Madsen, E., Hobson, M., Shi, H., Varghese, T. and Frank, G. (2005). Tissue-mimicking agar/gelatin materials for use in heterogeneous elastography phantoms. Physics in Medicine and Biology, 50(23), pp.5597-5618.

[93] R. Porto, "AgarGel : Agar-Agar : Properties and Specifications", Agargel.com.br, 2019. [Online]. Available: http://www.agargel.com.br/agar-tec-en.html. [Accessed: 26- Apr- 2019]

[94] Protocols Online. (2019). Lysogeny broth. [online] Available at: https://www.protocolsonline.com/recipes/media/lysogeny-broth/ [Accessed 4 May 2019].

APPENDIX

Appendix A: Code for ultrasound sensor using Arduino

```
const int echoPinT = 3;
const int trigPin = 9;
const int echoPinR = 10;
long duration, distanceCm;
int Status;
void setup()
{
  pinMode(trigPin, OUTPUT);
  pinMode(echoPinT, INPUT);
  pinMode(echoPinR, INPUT);
  Serial.begin(9600);
}
void loop()
{
  Status = Serial.read();
  if (Status == 1)
  {
    digitalWrite(trigPin, LOW);
    delayMicroseconds(2);
```

```
   digitalWrite(trigPin, HIGH);
   delayMicroseconds(10);
   digitalWrite(trigPin, LOW);
   duration = pulseIn(echoPinR, HIGH);
   distanceCm = duration * 0.01725;
  Serial.println(distanceCm);
   delay(500);
  }
 else if (Status == 0)
 {
   Serial.print("Stopping....");
 }
 else
 {
   Serial.print("Wrong Input.... Press '1' to Start and '0' to Stop");
 }
}
```

Appendix B: Software developed for importing Serial Monitor data into an Excel file

The lack of free and easy to use software to extract the data from the Arduino serial monitor led me to develop a software that can do this. The software is the byproduct of combining parts of codes from different Open Source Software. The software was build using Microsoft Visual Studio and a .exe file was produced so that this software can be run on any Windows system. Below is a screenshot of the screen (also Figure 3.2). When the Arduino is connected to the computer, choose the device from the drop-down populated for 'Select a port' and choose the Baud rate. Once 'Connect' is pressed, the software connects to the Arduino. If the device is not found, it will display an error.

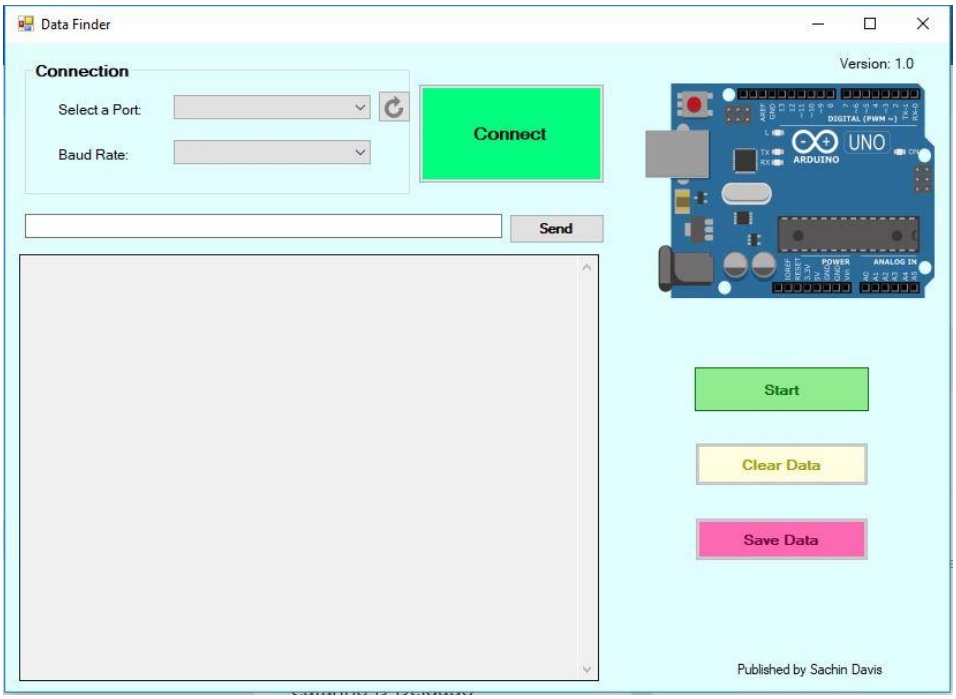

The software has a serial monitor where the data can be viewed in real-time and communication to the Arduino is achieved using the dialog box and ‘Send’ button. Once Start is pressed, the data begins displaying on the serial monitor. To export this data onto an Excel file, click on ‘Save Data’. This opens a dialog box where the location for the file can be selected and a name for the file can be chosen. In the first revision of this software (which is now available), the user must enter the filename with the extension i.e. If the user wants to save the data into an Excel file called ‘Present Data’, the user must type ‘Present Data.xlsx’ in the Save Dialog box. The serial monitor can be cleared by clicking on Clear Data.